ACADÉMIE
DES SCIENCES
INSTITUT DE FRANCE

Comptes Rendus
Chimie

Abdelatif Messaoudi and Pierre Braunstein

DFT investigations of 2D raft-type heterometallic clusters [MMoCp(or $C_5H_4NMe_2$)$(CO)_3]_n$ with triangular ($n = 3$) or square ($n = 4$) Cu, Ag, or Au metal cores

Volume 29 (2026), p. 279-301

Online since: 11 June 2026

https://doi.org/10.5802/crchim.448

The Comptes Rendus. Chimie *are a member of the Mersenne Center for open scientific publishing*
www.centre-mersenne.org — e-ISSN : 1878-1543

ACADÉMIE DES SCIENCES
INSTITUT DE FRANCE

Comptes Rendus. Chimie
2026, Vol. 29, p. 279-301
https://doi.org/10.5802/crchim.448

Research article

DFT investigations of 2D raft-type heterometallic clusters $[MMoCp(or\ C_5H_4NMe_2)(CO)_3]_n$ with triangular ($n = 3$) or square ($n = 4$) Cu, Ag, or Au metal cores

Abdelatif Messaoudi [*, a] **and Pierre Braunstein** [*, b]

[a] Laboratory of Materials Chemistry and the Living: Activity & Reactivity (LCMVAR), Department of Chemistry, Faculty of Matter Sciences, University of Batna 1, Batna, Algeria

[b] Institut de Chimie (UMR 7177 CNRS), Université de Strasbourg, 4 rue Blaise Pascal, CS 90032, Strasbourg Cedex F-67081, France

E-mails: amessaoudi@univ-batna.dz (A. Messaoudi), braunstein@unistra.fr (P. Braunstein)

Abstract. We present theoretical investigations of 2D raft-type heterometallic clusters $[MMoCp(or\ C_5H_4NMe_2)(CO)_3]_n$ (M = Cu, Ag, Au) with a triangular (n = 3) or square (n = 4) copper, silver, or gold core edge-bridged by three or four metalloligands $MoCp(or\ C_5H_4NMe_2)(CO)_3$, respectively (Cp = η^5-C_5H_5; $C_5H_4NMe_2$ = η^5-$C_5H_4NMe_2$). Various molecular symmetries, C_1, C_s, C_2, D_2, and S_4, were considered, and our calculations reveal an excellent agreement between the most stable computed structures and those determined experimentally by X-ray diffraction when the Cp ligand is used. In contrast, clusters incorporating the $C_5H_4NMe_2$ ligand display alternative geometries that are energetically more stable than those found experimentally, emphasising the crucial role of the π-bound ligand on cluster stability. For M = Cu, we demonstrate that square cores with elongated Cu–Cu distances can be stabilised, consistent with previously described systems. Energy decomposition analysis (EDA) at the BP86 level shows that the Cu, Ag, and Au clusters are stabilised by a strong interplay of electrostatic and orbital interactions, with markedly stronger binding in the tetranuclear systems due to cooperative metal–metal and metal–ligand effects. Frontier molecular orbital analysis was used to investigate the electronic structure and potential reactivity of these clusters. The results reveal that metal nature, NMe_2 substitution, and cluster nuclearity strongly affect the HOMO–LUMO gaps and charge-transfer behaviour. NMe_2-substituted Cu and Au clusters with higher nuclearity display reduced HOMO–LUMO gaps and greater frontier orbital delocalisation, indicating an increased propensity for redox processes. Our theoretical study satisfactorily reproduces the experimental structures of these 2D raft-type heterometallic clusters and highlights the possibility of uncovering new potentially accessible geometries of transition-metal clusters.

Keywords. Metal–metal bonds, Transition-metal clusters, Heterometallic clusters, Optimised geometries, Coinage metals, DFT calculations, d^{10}–d^{10} interactions.

Note. Part of the PhD thesis of AM, Université Louis Pasteur, Strasbourg (France), 2006 (national thesis number 2006STR13203).

Manuscript received 19 December 2025, revised 19 February 2026 and 16 March 2026, accepted 20 March 2026, online since 11 June 2026.

* Corresponding authors

Dedicated to Prof. Rick D. Adams, who has been a leader in the field of organometallic chemistry for over forty years, in particular in cluster chemistry, where he has made numerous outstanding contributions. He has beautifully served as Editor-in-Chief for the Journal of Organometallic Chemistry for twenty-seven years.

1. Introduction

After the pioneering report of Nyholm and coworkers of a heterometallic complex containing a direct metal–metal bond between a group 11 metal in the +I oxidation state (namely Cu(I), Ag(I), or Au(I)) and another transition metal in 1964 [1], a new research area developed in organometallic chemistry dedicated to the study of heterometallic bonds, and numerous relevant transition metal dinuclear and cluster complexes have since been synthesised and characterised with 1D, 2D, or 3D structures [2–7]. Notably, several metal clusters were found to display short intermetallic contacts between group 11 centres that challenged the conventional understanding of metal–metal bonding and were interpreted as evidence for d^{10}–d^{10} metallophilic interactions, a phenomenon that continues to attract significant attention due to its implications in bonding theory, structural diversity, and photophysics, with potential applications in material sciences [8–17]. Longoni and collaborators have described octanuclear, tetraanionic clusters $[NMe_3CH_2Ph]_4[Ag_4\{Fe(CO)_4\}_4]$ [18] and $[NEt_4]_4[Au_4\{Fe(CO)_4\}_4]$ [19], in which all Ag–Ag and Au–Au bonds are bridged by the formally dianionic metalloligand μ-$[Fe(CO)_4]$ (Scheme 1). The inner core of the Ag_4Fe_4 cluster adopts a square geometry, with Ag–Ag distances ranging from 3.036(1) to 3.334(1) Å. In contrast, the corresponding Au_4Fe_4 clusters display either a square (2.973(2), 2.831(2) Å) or a rectangular arrangement (2.932(2) and 3.400(2) Å) of gold atoms.

Furthermore, Klüfers et al. reported a series of clusters in which a central square of silver or copper atoms is stabilised by the formally monoanionic bridging metalloligand μ-$[Co(CO)_4]$ [20–22]. These diverse structures illustrate the ability of group 11 metals to assemble into highly symmetric frameworks when supported by carbonyl-based metalloligands. In contrast to these square arrangements, a triangular Cu_3 core, with an average Cu–Cu separation of 2.602 Å, was later characterised in the hexanuclear, trianionic cluster $[NEt_4]_3[Cu_3\{Fe(CO)_4\}_3]$ [23], in which the copper atoms are interconnected by μ-$[Fe(CO)_4]$ units (Scheme 2). The characterisation of the triangular Cu_3 and square Ag_4/Cu_4 systems highlights the structural versatility of group 11 closed-shell clusters, underscoring the delicate balance between electronic and steric effects that determines their nuclearity and overall structure.

Recent work has reported an unprecedented case of polymerisation isomerism in heterobimetallic carbonyl clusters $[\{MFe(CO)_4\}_n]^{n-}$ (M = Cu, Ag, Au; n = 3, 4), where triangular and square nuclearities coexist for the same elemental composition. Depending on the synthetic protocol, Ag and Au systems selectively form either trinuclear or tetranuclear clusters, whereas Cu stabilises only the triangular form. This behaviour has been rationalised by a balance between Fe–M bonding and metallophilic interactions, as revealed by structural and AIM analyses [24].

Our group reported a series of hexa- and octanuclear heterometallic clusters with a central core displaying d^{10}–d^{10} interactions, obtained by reaction of the carbonylmetallate $[Mo(C_5H_4NMe_2)(CO)_3]^-$ with $[Cu(NCMe)_4]PF_6$, $AgBF_4$, or $(NBu_4)[AuBr_2]$, respectively. These clusters were shown by X-ray diffraction to possess a triangular copper core in $[Cu_3\{Mo(C_5H_4NMe_2)(CO)_3\}_3]$ **A1**, and a square silver or gold core in $[Ag_4\{Mo(C_5H_4NMe_2)(CO)_3\}_4]$ **A2** and $[Au_4\{Mo(C_5H_4NMe_2)(CO)_3\}_4]$ **A3**, respectively (Scheme 3) [17,25–27].

Using the anion $[MoCp(CO)_3]^-$ (Cp = η_5-C_5H_5) had previously yielded similar clusters, with a triangular copper core in $[Cu_3\{MoCp(CO)_3\}_3]$ **A4**, and a square silver or gold core in $[Ag_4\{MoCp(CO)_3\}_4]$ **A5**, and $[Au_4\{MoCp(CO)_3\}_4]$ **A6**, respectively (Scheme 4) [25,26].

Combined experimental and theoretical investigations on clusters **A4–A6** demonstrated that the structural preference arises from the delicate balance between steric effects, ligand coordination modes, and d^{10}–d^{10} metallophilic interactions between the closed-shell metal centres [25,26]. These findings provided important insight into the role of metallophilic interactions in governing the geometry and stability of such heterometallic carbonyl clusters. In the present work, we extend this investigation to related systems incorporating the substituted metalloligand $[Mo(C_5H_4NMe_2)(CO)_3]^-$ in order to evaluate the influence of ligand functionalisation on the

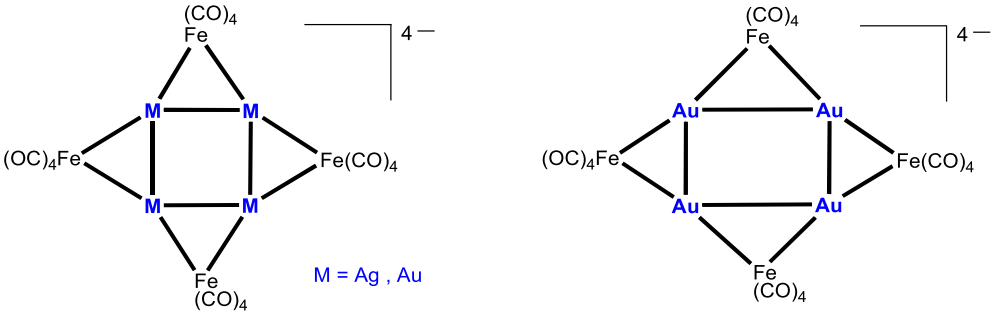

Scheme 1. Square or rectangular M_4 core in Ag_4Fe_4 and Au_4Fe_4 clusters [6,7,17,19].

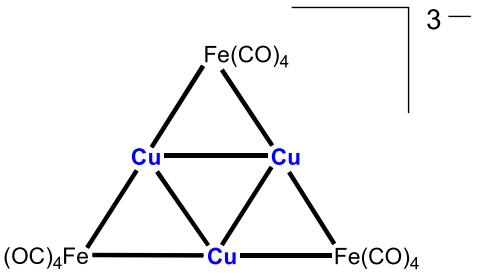

Scheme 2. Triangular structure of the Cu_3Fe_3 cluster [23].

structure and electronic properties of the resulting clusters.

The reason for introducing the $C_5H_4NMe_2$ ligand instead of Cp in the metal carbonyl fragment was to examine its potential influence on the nature and/or structure of the resulting clusters. Because a bridging bonding mode of the ligand $C_5H_4NMe_2$ has been demonstrated earlier in the heterodinuclear complex [Pt{Mo(μ-$C_5H_4NMe_2$)$(CO)_3$}(NCPh)Cl] (Mo–Pt) **B** [28] (Scheme 5), it was conceivable that the NMe_2 donor group could engage in bonding with an adjacent group 11 metal centre in the clusters of type **A** investigated here. Although this situation was not observed, the $C_5H_4NMe_2$ ligand in clusters **A1–A3** was found to influence the orientation of the metalloligand with respect to the central metal core and the overall molecular structure.

In clusters **A1–A6**, the bonding behaviour of the metalloligands $[MoCp(CO)_3]^-$ and $[Mo(C_5H_4NMe_2)(CO)_3]^-$ with respect to the d^{10}–d^{10} metal–metal bond is that of an anionic μ_2-unit bridging the M(I)–M(I) centres, acting formally as four-electron donors, which confers the usual 14-electron count to the coinage metals. This bridging bonding mode was observed for the first time in the centrosymmetric butterfly clusters [Pd_2(or Pt_2){$MoCp(CO)_3$}$_2$(PR_3)$_2$] [29–31] (Scheme 6).

Although the structures of these centrosymmetric metal clusters did not follow the original Wade–Mingos rules [32,33], they could be readily explained by considering that the d^9–d^9 M′–M′ bond was doubly bridged by the carbonylmetallates formally acting as four-electron donor anions, like μ_2-halides. This analogy was extended to the even rarer μ_3-bonding mode, first encountered in a Pd_3Mo cluster, where the carbonylmetallate could be viewed as an anionic six-electron donor, like a μ_3-halide [34] This electron-counting approach was subsequently successfully extended to isoelectronic or isolobal analogues of these carbonylmetallates [35].

In each of the clusters **A1**–**A6**, the short M–M distances provide clear evidence for the occurrence and stabilising role of metallophilic interactions between the closed-shell metal centres. To gain a deeper insight into the bonding in these systems, we carried out a detailed theoretical investigation aimed at elucidating the reasons for the stabilisation of specific structural motifs. Our study was designed to address two key aspects: (i) to rationalise the preference for the observed geometries of the six clusters under consideration, and (ii) to evaluate the relative stability of structures with different possible symmetries. DFT calculations have allowed us not only to reproduce the structural features observed experimentally but also to better understand the electronic factors underpinning their stability and structural diversity.

2. Computational details

All quantum chemical calculations were carried out using the TURBOMOLE software package [36].

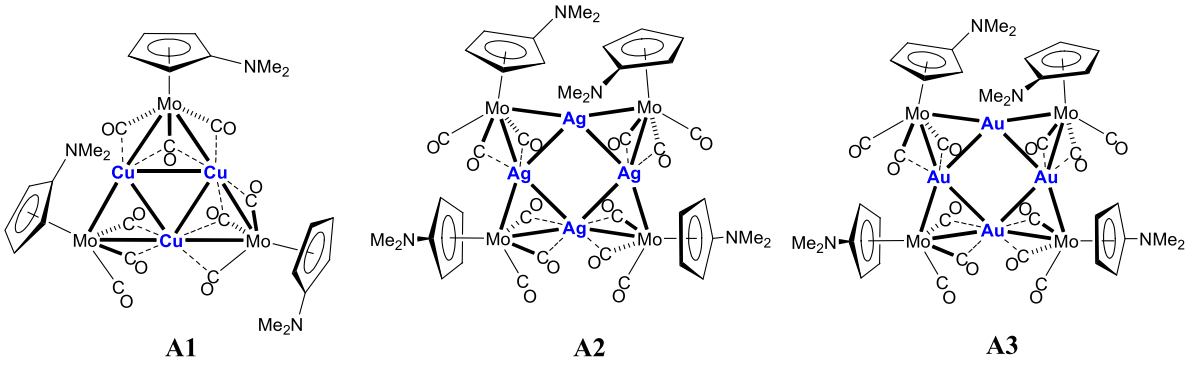

Scheme 3. Clusters $[MMo(C_5H_4NMe_2)(CO)_3]_n$ with a triangular copper ($n = 3$) or square silver or gold central core ($n = 4$).

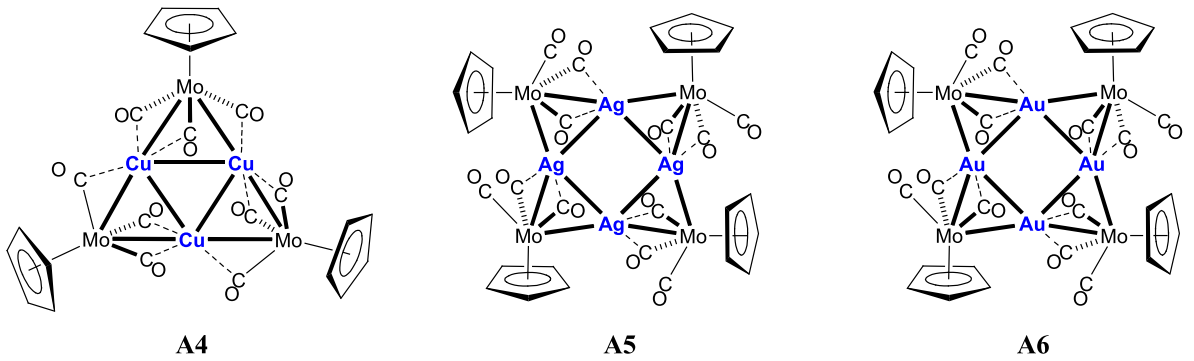

Scheme 4. Clusters $[MMoCp(CO)_3]_n$ with a triangular copper ($n = 3$) or square silver or gold central core ($n = 4$).

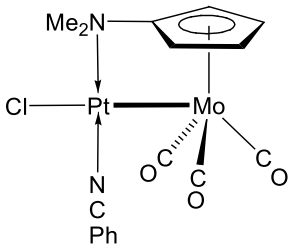

Scheme 5. Complex **B** with a bridging $C_5H_4NMe_2$ ligand [28].

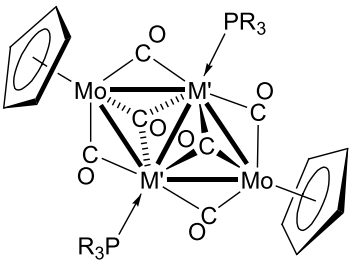

M' = Pd, Pt

Scheme 6. Centrosymmetric clusters of type **C** with centrosymmetric Mo_2Pd_2 or Mo_2Pt_2 core.

The BP86 density functional (Becke–Perdew86) was selected because of its proven reliability in describing diverse bonding situations, including those involving transition-metal complexes [37–39]. This choice further enabled the use of the efficient RI–J approximation for the treatment of Coulomb two-electron integrals [40–42]. For geometry optimisations, SV(P) basis sets were employed [43] consisting of a single basis function for core orbitals, a double-ζ description for the valence shells, and one set of polarisation functions for all atoms except hydrogen. To refine the electronic energies, single-point calculations were performed using the larger triple-ζ valence plus polarisation (TZVP) basis sets [44]. Stationary points on

the potential energy surface were verified through vibrational frequency analyses at the BP86/SV(P) level: minima were confirmed by the absence of imaginary frequencies, whereas the presence of a single imaginary frequency identified transition states [45–47]. In addition to Born–Oppenheimer potential energies (E, corrected for zero-point vibrational effects), Gibbs free energies (G) were also evaluated. Unless otherwise specified, all reported G values correspond to standard conditions of 25 °C and 1 bar CO, consistent with the experimental setup [26]. Energy decomposition analysis (EDA), originally developed by Morokuma [47], was employed to investigate the nature and origin of the interactions between the metal cores M_n (M = Cu, Ag, Au; $n = 3, 4$) and the metalloligand fragments $[MoCp(or\ C_5H_4NMe_2)(CO)_3]_n$ in the triangular ($n = 3$) and square ($n = 4$) heterometallic clusters. The EDA calculations were carried out using the Amsterdam modeling suite (AMS) [48]. Single-point EDA calculations were performed at the BP86/TZP level on geometries optimised at the BP86/SVP level with Turbomole. Within this formalism, the total interaction energy ΔE_{int} between the interacting fragments is decomposed into physically meaningful contributions according to Equation (1):

$$\Delta E_{int} = \Delta E_{Pauli} + \Delta E_{elstat} + \Delta E_{orb} \quad (1)$$

where ΔE_{Pauli} represents the Pauli repulsion arising from the overlap of occupied orbitals, ΔE_{elstat} corresponds to the classical electrostatic interaction between the unperturbed charge distributions of the fragments, and ΔE_{orb} accounts for the stabilising orbital interactions, including polarisation and charge-transfer effects that occur upon relaxation of the fragment densities [49]. All frontier-molecular-orbital (FMO) calculations were performed using the BP86 functional in combination with the def2-TZVP basis set [50–52], as implemented in the Gaussian 16 package [52].

3. Results and discussion

3.1. *Optimised geometries of the metal cores*

The main results from the computationally optimised geometries and the structures determined by X-ray diffraction of clusters **A1**–**A6** are presented and compared below. A detailed compilation of structural parameters, including bond lengths and bond angles, available in Tables S1–S6 in the Supporting Information, provide insights into the reliability of the theoretical methods employed.

3.1.1. *Clusters with a copper core*

In the structure of cluster **A1**, optimised in C_1 symmetry, the calculated Cu–Cu bond distances are 2.642, 2.580, and 2.531 Å, shorter than the experimental values by only 0.013, 0.036, and 0.048 Å, respectively, while the calculated Cu–Mo distances are longer by about 0.03 Å. A noticeable difference concerns the bridging carbonyl groups, where the calculated Cu–C bond lengths are shorter by up to 0.117 Å compared to the experimental values. The calculated bond angles match well the experimental data, with only small differences of 3.94°, 4.12°, 3.80°, and 3.01° for Mo(2)–C(1)–O(1), Mo(2)–C(11)–O(4), Mo(3)–C(21)–O(7), and Mo(3)–C(23)–O(9), respectively.

The X-ray diffraction study revealed that cluster **A4** with a triangular copper core crystallises in two different systems, triclinic and orthorhombic. The main difference between them lies in the presence of a triply bridging carbonyl group in the orthorhombic form. For both systems, geometry optimisation yielded similar structures, with the Cp and carbonyl ligands arranged in an overall C_3-symmetric orientation. For our study, we considered cluster **A4** in its orthorhombic crystalline form. The optimised Cu–Cu distances are, on average, shorter by 0.05 Å compared to those determined by X-ray diffraction. As in the case of cluster **A1**, slight deviations from the experimental values are observed in the calculated bond angles Mo(1)–C(3)–O(3), Mo(2)–C(7)–O(7), Mo(3)–C(4)–O(4), and Mo(3)–C(6)–O(6) of 3.36°, 3.49°, 3.95°, and 4.86°, respectively.

3.1.2. *Clusters with a silver or gold core*

The geometries of clusters **A2** and **A3** with a silver and gold square core, respectively, were optimised in C_2 symmetry. Compared to the experimental values, the calculated metal–metal distances are longer by about 0.04 Å in the silver square and by 0.12 Å in the gold square. Furthermore, the diagonal distances in the gold cluster are clearly overestimated, with a calculated Au(1)–Au(3) distance of 4.151 Å against 3.875 Å determined experimentally. In contrast, the M–Mo distances are in good agreement, with a maximum deviation of 0.04 Å for silver and 0.10 Å for gold. For the bridging carbonyl ligands, more pronounced

discrepancies are observed between the calculated and experimental values. For instance, in the case of silver, the Ag(2)–C(1) distance is longer by 0.16 Å while the Ag(2)–C(2) distance is shorter by 0.05 Å. This effect is even more pronounced in the gold square, where the Au(2)–C(2) distance decreases by 0.12 Å, while another Au–C bond length increases by 0.37 Å (Table S3). A significant structural difference between the silver- and gold-containing clusters lies in the Au–CO bonds being shorter than the corresponding Ag–CO bonds. Nevertheless, the calculated bond angles are in good agreement with the experimental values. The differences in bond lengths and angles sometimes observed between calculated and experimental values involving the coinage metals and CO ligands can be explained by the relative weakness of these interactions and their soft energy profile compared to the Mo–CO interactions; it is mostly the orientation of the $Mo(CO)_3$ cone that defines the position of the CO ligands with respect to the coinage metals [53,54].

After discussing the $C_5H_4NMe_2$ derivatives (**A2** and **A3**), we now turn to their Cp analogues, **A5** and **A6**, which display notable structural differences in the arrangement of their metal cores.

The silver square in **A5** and the gold square in **A6** exhibit significant differences in the arrangement of their atoms. For the geometry optimisation of cluster **A5**, it was necessary to impose a constraint, under C_2 symmetry, by arbitrarily fixing the torsion angle Ag(1)–Ag(2)–Ag(1a)–Ag(2a) at 21°, since unconstrained optimisation led to a planar square structure like that of the gold cluster, thereby causing convergence issues. The calculated Ag–Ag distances show a maximum elongation of about 0.07 Å. A significant difference is also observed for the diagonal distances, with calculated Ag(1)–Ag(1a) of 4.00 Å compared to 3.50 Å in the experimental structure, while calculated Ag(2)–Ag(2a) is shorter by 0.35 Å. Moreover, a pronounced discrepancy is found in the bond angles, with calculated values for Ag(1)–Ag(2)–Ag(1a) and Ag(2)–Ag(1)–Ag(2a) of 87.41° and 88.76°, compared to the experimental values of 75.92° and 100.23°, respectively.

In the structure of cluster **A6**, the four gold atoms are coplanar, and the diagonal distances are nearly identical, with Au(1)–Au(3) at 3.940 Å and Au(2)–Au(4) at 3.904 Å (Table S6). In contrast, the diagonal distances are very different in **A5** for Ag(1)–Ag(1a) and Ag(2)–Ag(2a) at 3.530 and 4.405 Å, respectively. Like in **A5**, the four Cp ligands and the carbonyl groups in **A6** adopt a similar orientation, consistent with an approximate S_4 symmetry (Table S5). When the geometry optimisation of cluster **A6** was started from C_1 symmetry, it converged to a geometry close to S_4 symmetry. The calculated Au–Au bond lengths are overestimated by up to ca. 0.15 Å compared to the experimental data. Nevertheless, the overall set of calculated distances is in satisfactory agreement with the experimental data, thereby validating the DFT method and basis set employed.

3.2. *Relative stabilities of the various models as a function of their molecular symmetry*

To better understand the relative stabilities of the different cluster architectures, we carried out geometry optimisations using DFT at the BP86 level of theory combined with the SV(P) basis set and explored, for each system, several possible symmetries, namely C_2, D_2, S_4, C_1, and C_s, to identify the most stable configuration.

The optimised geometries of the clusters containing the $C_5H_4NMe_2$ ligands are presented in Figure 1, while the corresponding structures with unsubstituted Cp ligands are displayed in Figure 2. This distinction allows a direct comparison of the effect of the NMe_2 substituent on the cluster stability and geometry.

For the eight-metal-atom clusters, the initial geometries were constructed on the basis of the experimental data for the related silver and gold square-type clusters. Specifically, we started from C_2 symmetry for the clusters containing the $C_5H_4NMe_2$ ligands, whereas we started from S_4 symmetric geometries for those containing the Cp ligands. To complement these models, we also examined hypothetical structures of D_2 symmetry (see structures **A8**–**A10** in Figure 1 and **A25**–**A27** in Figure 2), which provided useful comparisons.

3.2.1. *Cu-containing clusters*

3.2.1.1. With the $C_5H_4NMe_2$ ligands. For the hexanuclear clusters, the optimisations were guided by experimental observations. The geometries of the $C_5H_4NMe_2$-containing clusters were optimised starting from C_1 symmetry, while for the Cp analogues

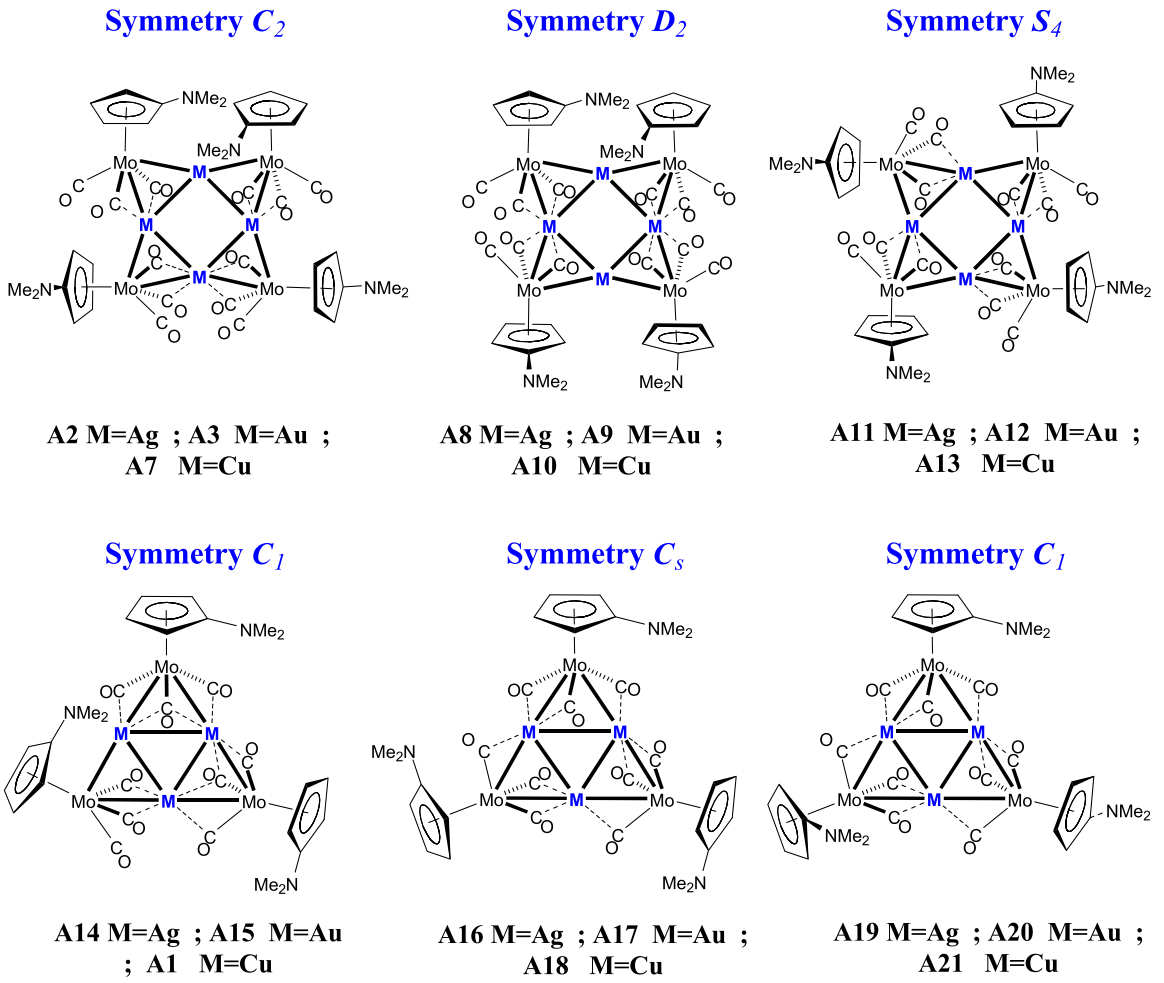

Figure 1. Optimised DFT/BP86 structures of the $[M_4\{Mo(C_5H_4NMe_2)(CO)_3\}_4]$ and $[M_3\{Mo(C_5H_4NMe_2)(CO)_3\}_3]$ clusters (M = Cu, Ag, Au) under different symmetry constraints (C_1, C_2, D_2, S_4, and C_s).

(see below), we adopted a slightly distorted C_1 geometry close to C_s symmetry. Furthermore, a hypothetical C_s-like model was considered, where the $C_5H_4NMe_2$ ligands are positioned on opposite sides of the metal plane (structures **A19**–**A21**, Figure 1). This configuration was introduced to probe the effect of the orientation of the aromatic ligand on the overall cluster stability and electronic distribution.

Overall, this systematic optimisation approach, covering multiple symmetries and both Cp and $C_5H_4NMe_2$ ligand types, provided a coherent framework for evaluating how the metal (Cu, Ag, Au) and the π-ligand substitution (Cp or $C_5H_4NMe_2$) affect the structural preferences and relative stabilities of these polymetallic clusters.

The relative energies and the calculated metal–metal bond distances for the different clusters optimised under the various symmetry constraints are compiled in Tables 1–4, which allows a direct comparison between the alternative structural models, highlighting the effect of symmetry on both the energetic stability and the geometric features of the clusters.

The optimisation of the three models with a copper square core led to distinct geometries. Cluster **A7**, with C_2 symmetry, converges to the same structure as that found for the silver square, displaying short Cu–Cu distances of 2.55 and 2.65 Å. In contrast, for clusters **A10** and **A13**, with D_2 and S_4 symmetry, longer Cu–Cu distances of 3.32 Å and 3.34 Å were obtained,

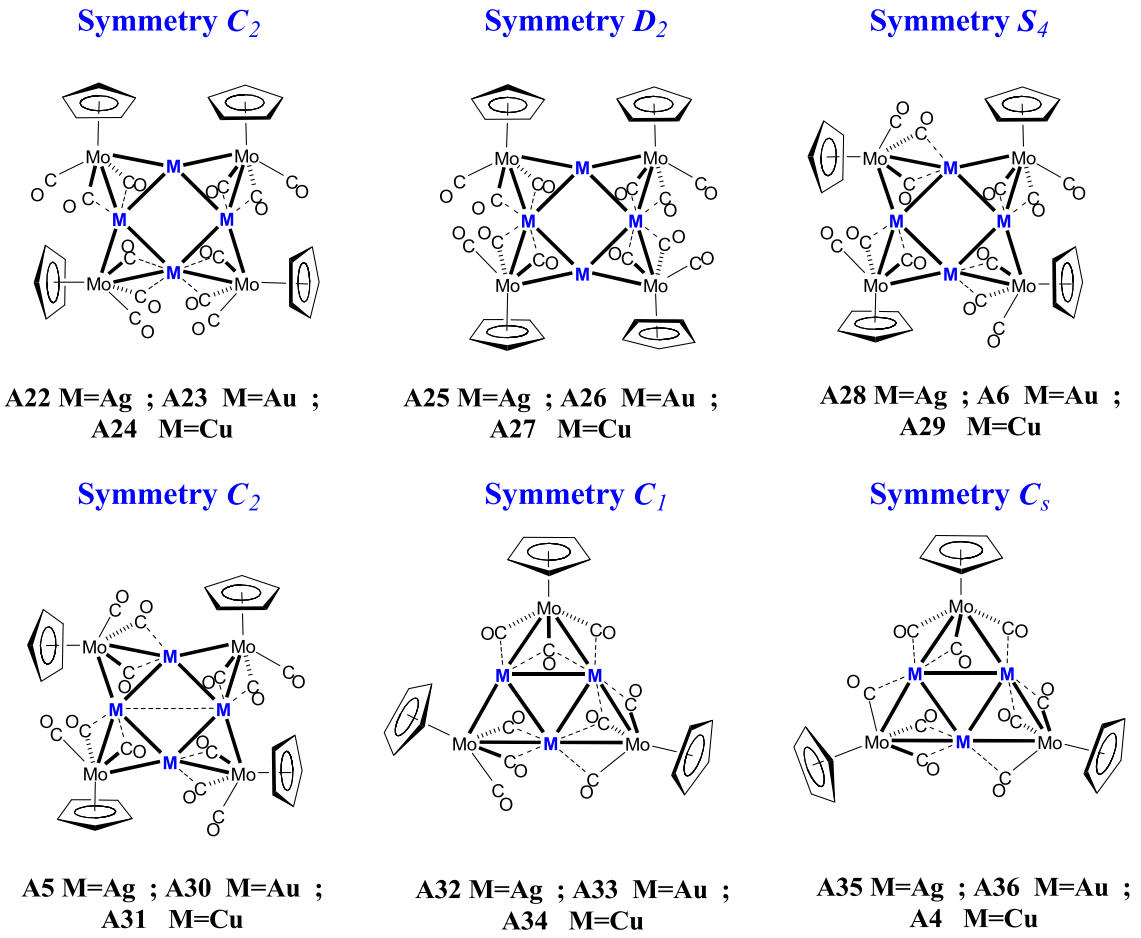

Figure 2. Optimised DFT/BP86 structures of $[M_4\{MoCp(CO)_3\}_4]$ and $[M_3\{MoCp(CO)_3\}_3]$ clusters (M = Cu, Ag, Au) under different symmetry constraints (C_1, C_2, D_2, S_4, and C_s).

Table 1. Main geometrical parameters (distances in Å) and relative energies (in Hartree and ΔE in kJ/mol) for the models $[Cu_4\{Mo(C_5H_4NMe_2)(CO)_3\}_4]$ and $[Cu_3\{Mo(C_5H_4NMe_2)(CO)_3\}_3]$, optimised under different symmetry constraints (C_1, C_2, D_2, S_4, and C_s)

Clusters	Symmetry	d^{10}–d^{10} Distances (Å)	E (Hartree)	ΔE (kJ/mol)
		$[Cu_4\{Mo(C_5H_4NMe_2)(CO)_3\}_4]$		
A7	C_2	2.55; 2.65	−9508.231	0
A10	D_2	3.32	−9508.249	−47.40
A13	S_4	3.34	−9508.252	−53.37
		$[Cu_3\{Mo(C_5H_4NMe_2)(CO)_3\}_3]$		
A1	C_1	2.58, 2.60, 2.64	−7131.182	0
A18	C_s	2.62	−7131.178	+10.18
A21	C_1	2.60	−7131.187	−12.72

Table 2. Main geometrical parameters (distances in Å) and relative energies (in Hartree and ΔE in kJ/mol) for the models $[Cu_4\{MoCp(CO)_3\}_4]$ and $[Cu_3\{MoCp(CO)_3\}_3]$, optimised under different symmetry constraints (C_1, C_2, D_2, S_4, and C_s)

Clusters	Symmetry	d^{10}–d^{10} Distances (Å)	E (Hartree)	ΔE (kJ/mol)
		$[Cu_4\{MoCp(CO)_3\}_4]$		
A24	C_2	2.58, 2.68	−8972.149	0
A27	D_2	2.52	−8972.140	+23.52
A29	S_4	2.75	−8972.159	−25.45
A31	C_2	2.70, 2.74	−8972.154	−13.74
		$[Cu_3\{MoCp(CO)_3\}_3]$		
A34	C_1	2.54, 2.55, 2.64	−6729.124	0
A4	C_s	2.60	−6729.127	−9.55

Table 3. Main geometrical parameters (distances in Å) and relative energies (in Hartree and ΔE in kJ/mol) for the models $[M_4\{Mo(C_5H_4NMe_2)(CO)_3\}_4]$ and $[M_3\{Mo(C_5H_4NMe_2)(CO)_3\}_3]$ (M = Ag or Au), optimised under different symmetry constraints (C_1, C_2, D_2, S_4, and C_s)

Clusters	Symmetry	d^{10}–d^{10} Distances (Å)	E (Hartree)	ΔE (kJ/mol)
		$[Ag_4\{Mo(C_5H_4NMe_2)(CO)_3\}_4]$		
A2	C_2	2.84, 2.94	−3533.290	0
A8	D_2	2.91	−3533.286	+10.44
A11	S_4	2.96	−3533.294	−10.92
		$[Ag_3\{Mo(C_5H_4NMe_2)(CO)_3\}_3]$		
A14	C_1	2.89, 2.95, 2.99	−2649.958	0
A16	C_s	3.01	−2649.958	+1.81
A19	C_1	2.98	−2649.962	−9.26
		$[Au_4\{Mo(C_5H_4NMe_2)(CO)_3\}_4]$		
A3	C_2	2.88, 2.93	−3488.520	0
A9	D_2	2.95	−3488.513	+17.25
A12	S_4	2.90	−3488.522	−7.063
		$[Au_3\{Mo(C_5H_4NMe_2)(CO)_3\}_3]$		
A15	C_1	2.96, 3.12, 3.18	−2616.377	0
A17	C_s	3.17	−2616.378	−2.25
A20	C_1	3.12, 3.13, 3.14	−2616.379	−6.20

respectively. Taking the energy of isomer **A7** as a reference, isomers **A10** and **A13** were found to be energetically more stable by 47.40 and 53.37 kJ/mol, respectively.

For the clusters with a triangular core **A1**, **A18**, and **A21**, geometry optimisation led to the same structural motif, with Cu–Cu distances in the 2.58–2.62 Å range. This results in a stabilisation of isomer **A21** by 12.72 kJ/mol and a destabilisation of isomer **A18** by 10.18 kJ/mol, relative to the experimentally observed structure of cluster **A1** (the energy of isomer **A1** being taken as the reference).

3.2.1.2. With the Cp ligands. In the case of the square copper clusters containing the Cp ligands, the Cu–Cu bond lengths are noticeably shorter

Table 4. Main geometrical parameters (distances in Å) and relative energies (in Hartree and ΔE in kJ/mol) for the models $[M_4\{MoCp(CO)_3\}_4]$ and $[M_3\{MoCp(CO)_3\}_3]$ (M = Ag or Au), optimised under different symmetry constraints (C_1, C_2, D_2, S_4, and C_s)

Clusters	Symmetry	d^{10}–d^{10} Distances (Å)	E (Hartree)	ΔE (kJ/mol)
		$[Ag_4\{MoCp(CO)_3\}_4]$		
A22	C_2	2.88, 2.95	−2997.209	0
A25	D_2	2.85	−2997.209	+0.92
A28	S_4	2.93	−2997.216	−18.14
A5	C_2	2.88, 2.92	−2997.212	−8.72
		$[Ag_3\{MoCp(CO)_3\}_3]$		
A32	C_1	2.88, 2.93, 3.02	−2247.901	0
A35	C_s	2.99	−2247.903	−4.38
		$[Au_4\{MoCp(CO)_3\}_4]$		
A23	C_2	2.91, 2.92	−2952.437	0
A26	D_2	2.90	−2952.434	+8.18
A6	S_4	2.91	−2952.442	−14.16
A30	C_2	2.89, 2.91	−2952.439	−7.12
		$[Au_3\{MoCp(CO)_3\}_3]$		
A33	C_1	2.94, 3.07, 3.22	−2214.317	0
A36	C_s	3.14	−2214.318	−1.56

than those obtained for the systems containing the $C_5H_4NMe_2$ ligand. For instance, cluster **A27** with D_2 symmetry exhibits Cu–Cu distances of approximately 2.52 Å, which are even shorter than the experimental values determined by X-ray diffraction. By contrast, cluster **A29** with S_4 symmetry displays d^{10}–d^{10} separations very similar to those observed in cluster **A31** with C_2 symmetry. Cluster **A29** was found to be more stable by 25.45 kJ/mol relative to **A24** taken as a reference and by nearly 50 kJ/mol compared to cluster **A27**. These results clearly indicate that the S_4-symmetric square arrangement represents the energetically most favourable configuration among the clusters containing a square copper core.

For the triangular copper clusters, the optimised geometries reveal that the Cu–Cu bond lengths vary slightly depending on the considered symmetry. In the case of cluster **A4** with C_s symmetry, the calculated Cu–Cu distances are uniform, around 2.60 Å. For cluster **A34** with C_1 symmetry, the Cu–Cu separations are more dispersed, ranging from 2.54 to 2.64 Å. From an energetic standpoint, cluster **A4** is more stable than cluster **A34** by 9.5 kJ/mol, suggesting that the C_s-symmetric triangular arrangement is energetically preferred over the C_1 variant. This stabilisation highlights the role of symmetry in determining the most favourable structural configuration for copper clusters containing a triangular core.

The energies calculated for clusters **A2** (M = Ag) and **A3** (M = Au), optimised from the experimental data, are used as reference values for the square systems, while the energies of clusters **A14** (M = Ag) and **A15** (M = Au) are arbitrarily chosen as reference values for the triangular systems.

3.2.2. *Ag- and Au-containing clusters*

3.2.2.1. With the $C_5H_4NMe_2$ Ligands. In contrast to what was observed for the square copper clusters, the geometry optimisation of the silver and gold square clusters yielded calculated distances close to the experimental values for all three symmetries, C_2, D_2, and S_4.

Cluster **A11** with S_4 symmetry, featuring an Ag–Ag distance of 2.96 Å, is more stable by 10.92 kJ/mol than

isomer **A2**, whereas cluster **A8** with D_2 symmetry is destabilised by 10.44 kJ/mol relative to **A2**. For the triangular clusters **A14**, **A16**, and **A19**, the calculated Ag–Ag distances range from 2.89 to 3.00 Å for **A14** and are around 3.00 Å for both **A16** and **A19**. Cluster **A19** is more stable than **A14** by 9.26 kJ/mol.

For the triangular and square gold clusters, results similar to those found for the silver clusters were obtained. The Au–Au distances in the triangular clusters are significantly longer than those in the square clusters, as exemplified by cluster **A15**, where the distances range from 2.96 to 3.18 Å. Among the square systems, the S_4-symmetric cluster **A12** is the most favourable, while in the triangular systems, the C_s-like symmetric cluster **A20** is preferred.

3.2.2.2. With the Cp ligands. We obtained similar results for the square silver clusters containing Cp or $C_5H_4NMe_2$ ligands. Cluster **A28** with S_4 symmetry is preferred by 18.14 kJ/mol over cluster **A22** with C_2 symmetry, and by 10.58 kJ/mol over cluster **A5**, also with C_2 symmetry.

For the triangular silver clusters, **A32** with C_1 symmetry exhibits different Ag–Ag distances of 2.88, 2.93, and 3.02 Å, while cluster **A35** with C_s symmetry shows Ag–Ag separations of about 2.99 Å. The latter is more stable by 4.38 kJ/mol compared to cluster **A32**. Similar observations can be made for the gold-containing clusters, where cluster **A6** with S_4 symmetry is the most favourable among the square systems. In contrast, the triangular clusters **A33** and **A36** are nearly isoenergetic; however, their optimisation leads to longer Au–Au distances, reaching up to 3.22 Å.

Overall, the stability of the clusters studied in this work is strongly influenced by both the nature of the coinage metal and the adopted symmetry, which is itself influenced by the NMe_2-substituent at the organic π-ligand. In the case of copper, short M–M contacts are favoured in square geometries, while triangular motifs show moderate stabilisation depending on symmetry. In the case of silver and gold, the optimised structures generally reproduce the experimental distances more closely, with S_4 symmetry emerging as the most stable for square clusters. For triangular clusters, the relative stabilisations are smaller, but optimisation often leads to elongated M–M distances, especially for gold. These trends highlight the key role of symmetry in dictating both geometry and relative stability across the series.

3.3. *Optimised geometries starting from elongated metal–metal distances*

Geometry optimisations were initiated from deliberately elongated metal–metal distances to avoid any predefined interaction. This approach allows an unbiased evaluation of whether a metal–metal bond is intrinsically favoured, with any contraction arising solely from the system's electronic effects. After examining the stability of the different models (**A1**–**A36**), we determined that the square copper clusters **A10** (D_2 symmetry), **A13** (S_4 symmetry), and **A29** (S_4 symmetry) are the most stable. The optimised structures of **A10** and **A13** display large Cu–Cu separations of 3.32 and 3.34 Å, respectively, and the molybdenum and copper atoms are coplanar. In these systems, each Cu–Mo–Cu unit contains one triply bridging carbonyl and two doubly bridging carbonyls (see Figure 3). In contrast, structure **A29** exhibits a shorter Cu–Cu distance of 2.75 Å, with the molybdenum atoms displaced out of the plane defined by the copper square, and the carbonyl ligands adopting only doubly bridging coordination modes. Furthermore, the orientation of the $C_5H_4NMe_2$ ligands in **A10** and **A13** differs markedly from that of the Cp ligands in **A29** (Figure 3).

We sought to optimise structures derived from models **A10** and **A13** with D_2 and S_4 symmetries, which exhibit large metal–metal distances for the three coinage metals, and Cp or $C_5H_4NMe_2$ ligands. In the case of the copper square, we successfully obtained two optimised structures, **A41** and **A42** (Figure 4), showing large Cu–Cu distances for the D_2 and S_4 symmetries with the Cp ligand. These results are comparable to those for structures **A10** and **A13** presented in Figure 3. In contrast, for silver and gold, the optimisation of the S_4 symmetric structures with both types of ligands yielded geometries with short M–M distances of about 2.75 Å for silver and 2.90 Å for gold. However, optimisation of the D_2 symmetric structures with both Cp or $C_5H_4NMe_2$ ligands led to geometries with large metal–metal separations, 3.38 Å and 3.44 Å for the silver squares **A37** and **A39**, and 3.54 Å and 3.56 Å for the gold squares **A38** and **A40** (Figure 4).

Optimisation attempts starting from elongated metal–metal separations show that only square copper clusters can retain such large Cu–Cu distances, while the silver or gold square clusters

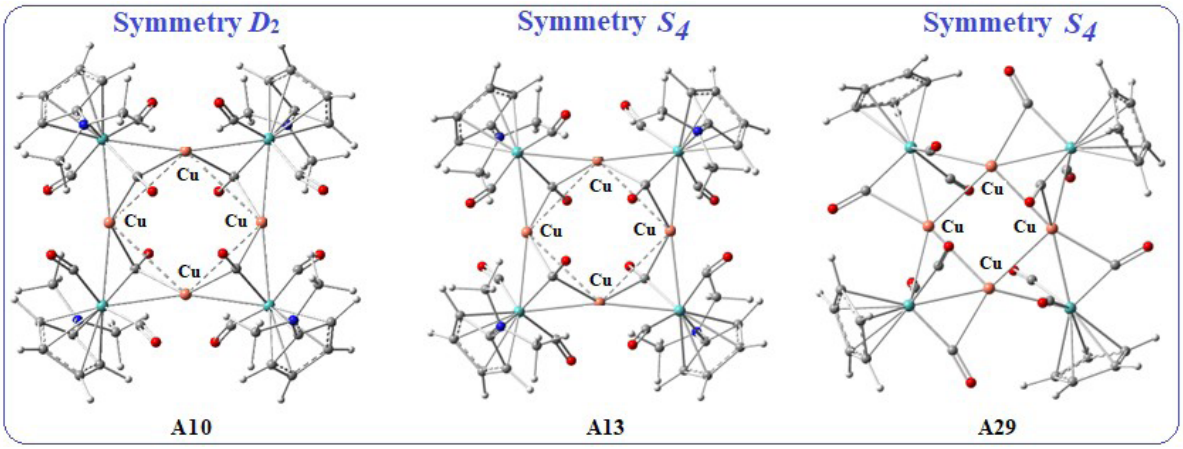

Figure 3. Optimised DFT/BP86 structures of **A10**, **A13**, and **A29**.

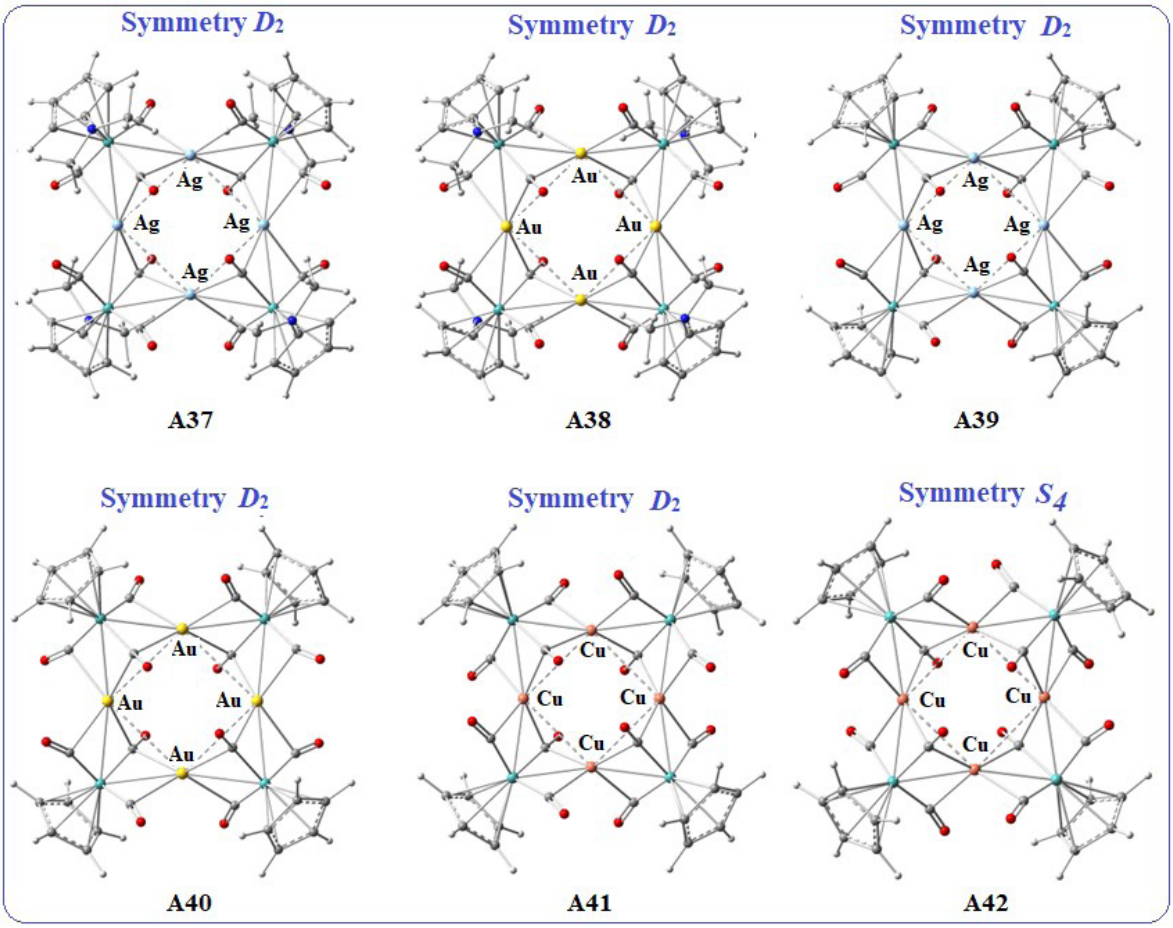

Figure 4. Clusters with silver, gold, and copper squares **A37**–**A41** with D_2 symmetry and **A42** with S_4 symmetry.

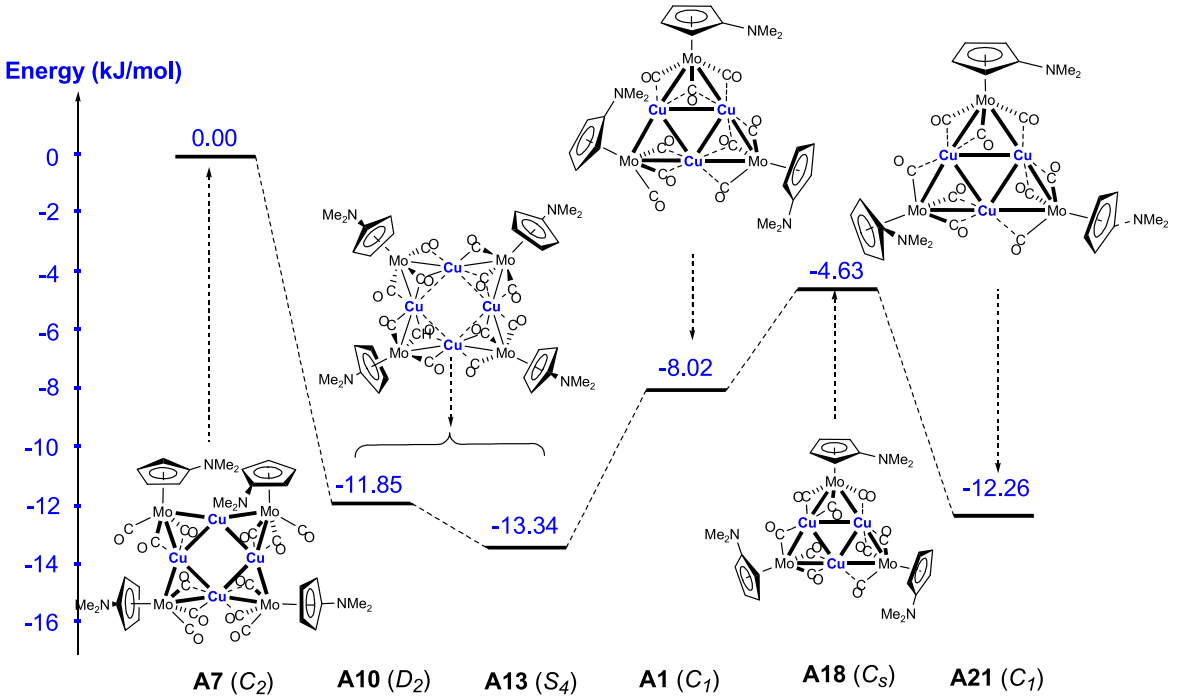

Figure 5. Relative energies (ΔE in kJ/mol) for the fragment Cu[Mo($C_5H_4NMe_2$)$(CO)_3$].

predominantly relax to shorter M–M bonds in S_4 symmetry. However, D_2 symmetric Ag and Au squares can retain elongated M–M distances, highlighting a clear dependence of the final geometry on both the metal type and cluster symmetry.

3.4. *Energies of the individual fragments MMo($C_5H_4NMe_2$)$(CO)_3$ and MMoCp$(CO)_3$ (M = Cu, Ag, Au)*

To complement the previous results and clarify further the structural preferences and relative stabilities of triangular and square clusters, we conducted a comparative analysis of the relative energies of the fragments MMo($C_5H_4NMe_2$)$(CO)_3$ and MMoCp$(CO)_3$ (M = Cu, Ag, Au), which constitute building blocks in the final clusters. For the square-type clusters, we normalised the total electronic energy by dividing it by four, considering the four constitutive fragments, while for the triangular-type clusters, the total energy was divided by three. This normalisation procedure, which allows a direct comparison between clusters with different nuclearities, follows the approach previously introduced in our earlier study [25]. As reference points, we used **A2**, **A3**, and **A7** for the MMo($C_5H_4NMe_2$)$(CO)_3$ systems, and **A22**–**A24** for the MMoCp$(CO)_3$ systems. The relative energies thus obtained provide a reliable basis for evaluating which geometries and symmetries are energetically more favourable. The resulting energy differences were plotted as energy diagrams (Figures 5–8), clearly illustrating stability trends across the coinage metals. These diagrams not only emphasise the energetic preferences of each system but also enable visualisation of the effect of ligand substitution (Cp or $C_5H_4NMe_2$) on cluster stability. Overall, this comparative study offers a consistent picture of how the interplay between the nature of the metal centre, the π-ligand, and the symmetry influences fragment stabilisation. The analysis of these relative energies is key to understanding the structural preferences of the copper-, silver-, and gold-containing clusters and will underpin discussions of their electronic properties in the following sections.

3.4.1. *Fragment Cu[Mo($C_5H_4NMe_2$)$(CO)_3$]*

The analysis shows that the square cluster **A13** with S_4 symmetry and the triangular cluster **A21** are energetically more favourable compared to the

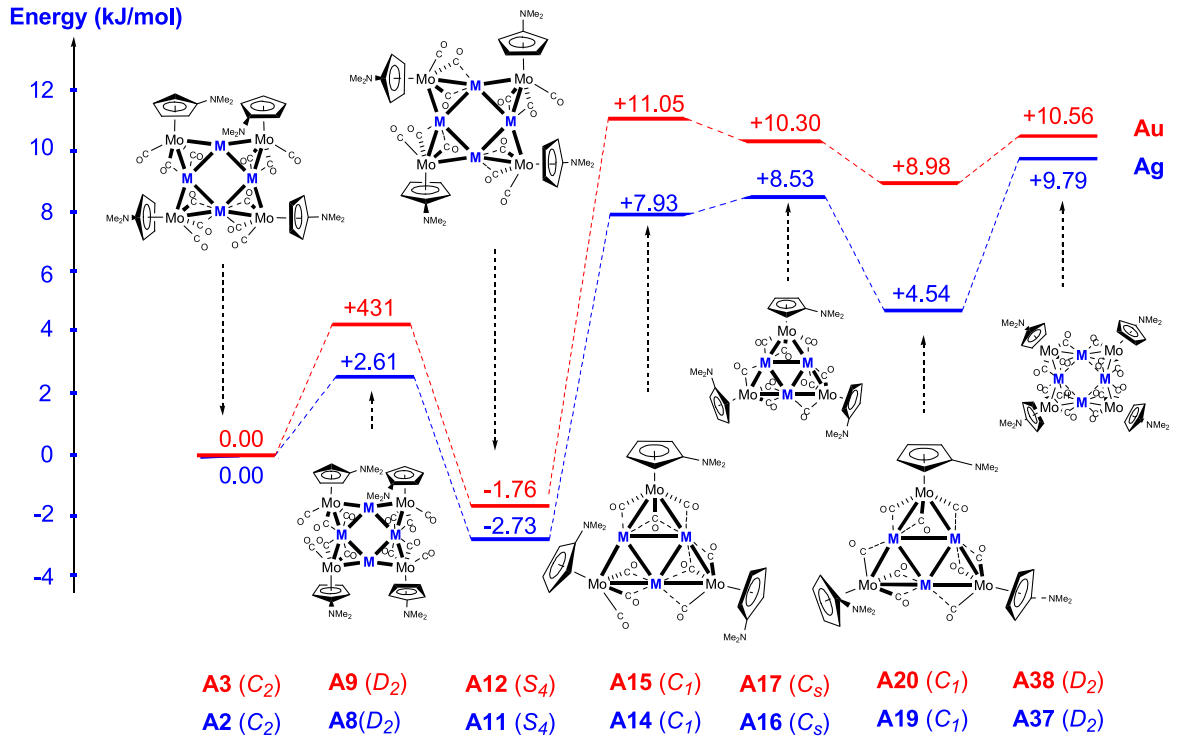

Figure 6. Relative energies (ΔE in kJ/mol) for the fragments M[Mo($C_5H_4NMe_2$)$(CO)_3$] (M = Ag and Au).

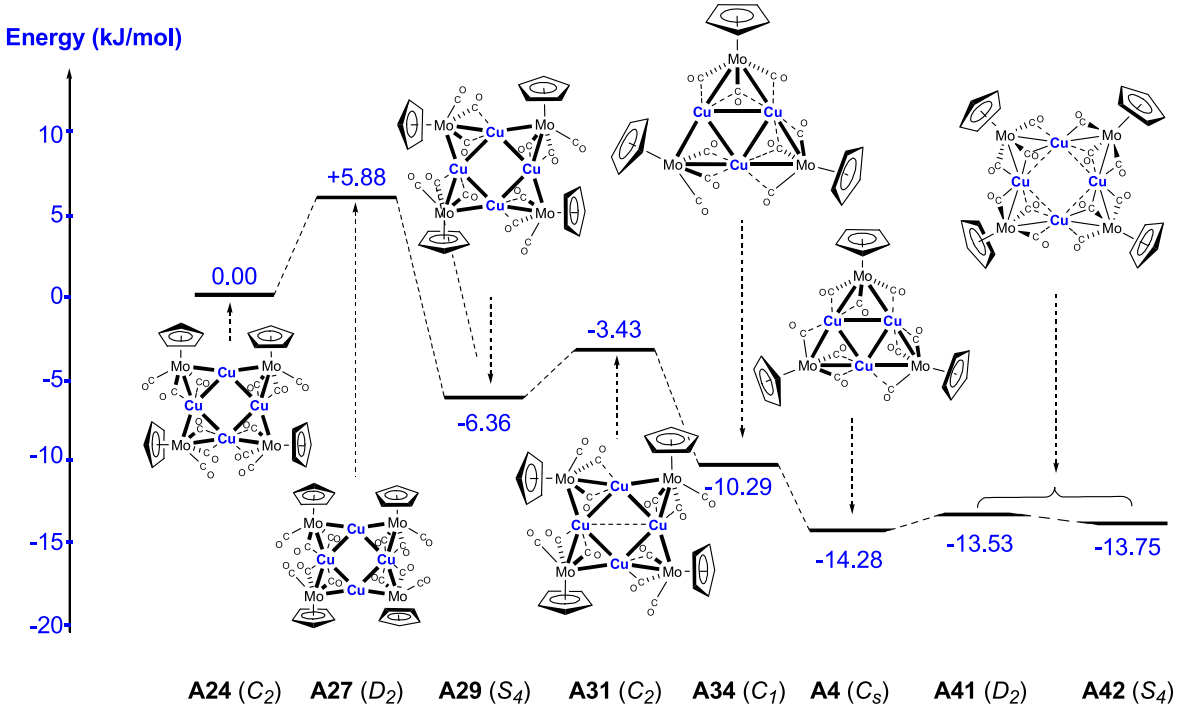

Figure 7. Relative energies (ΔE in kJ/mol) for the fragment Cu[MoCp$(CO)_3$].

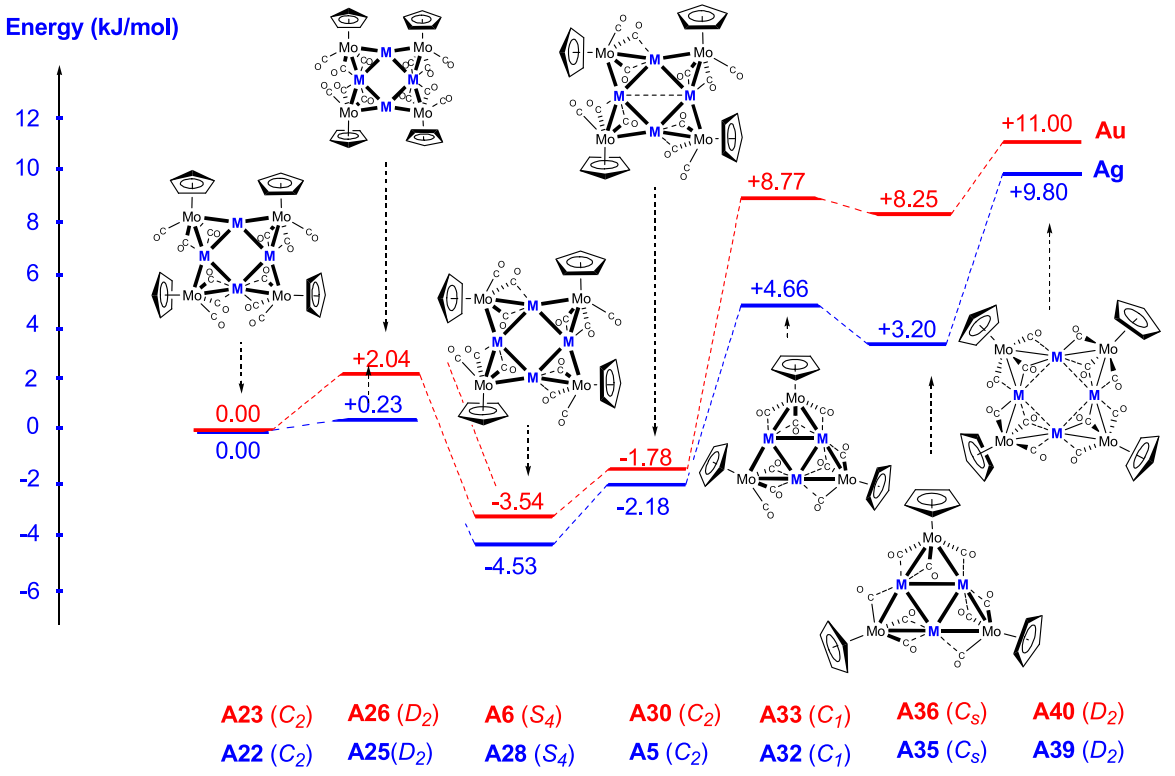

Figure 8. Relative energies (ΔE in kJ/mol) for the fragments M[MoCp(CO)$_3$] (M = Ag and Au).

experimentally observed structure **A1**. This energetic preference highlights an intrinsic tendency of copper to prefer the square rather than the triangular arrangement. However, this stabilisation is only achieved when the Cu–Cu separations are significantly elongated, with optimised distances around 3.30 Å. Such elongated Cu–Cu distances reduce the repulsive interactions within the metallic core and allow a better electronic distribution between the copper and molybdenum centres, thereby favouring the square geometry.

3.4.2. *Fragments M[Mo(C$_5$H$_4$NMe$_2$)(CO)$_3$] (M = Ag or Au)*

In contrast to the case of copper, the most stable silver and gold clusters with the $C_5H_4NMe_2$ ligands are the square clusters **A11** and **A12**, respectively, both adopting S_4 symmetry with short M–M distances.

The triangular structures **A14**–**A17**, **A19**, and **A20**, as well as the square structures **A37** and **A38** with elongated M–M separations, are less stable than **A2** and **A3**. The preference for shorter M–M distances in the case of silver and gold can be attributed to electronic and steric factors: shorter metal–metal distances maximise metal–metal interactions and allow a more favourable overlap with the CO ligands. Overall, these results highlight that, unlike with copper, silver and gold square arrangements with S_4 symmetry and short M–M separations are energetically preferred, emphasising the role of the intrinsic electronic properties of the coinage metal in determining the cluster stability.

3.4.3. *Fragment Cu[MoCp(CO)$_3$]*

In this case, the theoretical results are in excellent agreement with the experimental structures determined by X-ray diffraction, confirming that the triangular cluster **A4** indeed corresponds to the most stable arrangement for the copper-containing clusters. We also successfully obtained an optimised S_4-symmetric structure **A29**, featuring short Cu–Cu distances of approximately 2.75 Å. In this structure, the carbonyl ligands occupy positions very similar

to those observed experimentally in **A4**, demonstrating that the stereoelectronic environment is properly captured by the DFT calculations. The fragment corresponding to structure **A29** exhibits a stability comparable to that of the fragment from structure **A4**, and it is also more stable than the square structure **A42**, which has elongated metal–metal distances. These observations highlight that triangular arrangements are energetically favoured for copper when metal–metal distances are moderate, while square geometries with long Cu–Cu separations can also be stabilised under specific conditions. Overall, the results provide a coherent picture of the interplay between geometry, metal–metal distances, and ligand orientation in determining the relative stability of the copper-containing clusters (Figure 7).

Overall, the calculations confirm that the triangular copper cluster **A4** is the most stable, with a S_4-symmetric structure like **A29** where shorter Cu–Cu distances provide additional stabilisation, while square clusters with elongated metal–metal separations are less favoured.

3.4.4. *Fragments M[MoCp(CO)$_3$] (M = Ag or Au)*

In the case of silver-containing clusters, our calculations reveal a clear discrepancy with the experimental observations. Indeed, the fragment corresponding to the experimentally determined structure **A5** does not correspond to the most stable structure, since the fragment of the square structure **A28** with S_4 symmetry is more stabilised.

This suggests that, although the triangular geometry is accessible experimentally for silver, the square arrangement with short Ag–Ag distances is intrinsically more favourable from an energetic point of view. In contrast, for the gold cluster **A6**, the theoretical calculations are in perfect agreement with the experimental data obtained by X-ray diffraction. This concordance strongly supports the reliability of our computational approach and confirms that, unlike for silver, the triangular geometry experimentally observed for gold indeed corresponds to the most stable form.

3.5. *Bonding analysis*

Tables S6–S11 summarise the energy decomposition analysis (EDA) results for the interactions between the metal cores and the metalloligand fragments $[MoCp(CO)_3]_n$, calculated at the BP86 level. Here, ΔE_{int} denotes the total interaction energy, while ΔE_{elstat} and ΔE_{orb} correspond to the electrostatic and orbital (covalent) contributions, respectively. Energy decomposition analysis at the BP86 level was performed to elucidate the nature of the interactions between the Cu_n, Ag_n, and Au_n metal cores and the metalloligand fragments $[MoCp(CO)_3]_n$ and $[Mo(C_5H_4NMe_2)(CO)_3]_n$ for all investigated clusters. In every case, the strongly negative ΔE_{int} values indicate that cluster formation is governed by highly stabilising metal–ligand interactions.

The BP86 EDA results show that all Cu-based complexes are strongly stabilised by their interaction with the metalloligand fragments. The Cu_3 systems (**A1**, **A18**, and **A21**) exhibit interaction energies of around -4.93×10^3 kJ/mol, whereas the Cu_4 clusters (**A7**, **A10**, and **A13**) exhibit much larger stabilisations of -7.28 to -7.60×10^3 kJ/mol, highlighting the stronger binding in the square architectures. This difference mainly arises from the electrostatic term, which increases markedly when going from Cu_3 (-4.46 to -4.56 MJ/mol) to Cu_4 (-6.38 to -6.95 MJ/mol). The orbital contribution also becomes significantly more stabilising in the Cu_4 systems, indicating improved Cu–Mo covalency and more efficient metal–ligand orbital mixing. Although Pauli repulsion is larger in the more compact Cu_4 cores, it is clearly outweighed by the enhanced electrostatic and orbital attractions, resulting in superior overall stability of the tetranuclear complexes.

All Ag-containing systems display highly favourable interaction energies. The Ag_3 complexes (**A14**, **A16**, **A19**) show ΔE_{int} values close to -4.45 MJ/mol, while the Ag_4 species (**A2**, **A8**, **A11**, and **A37**) are much more stabilised, with values approaching -7.0 MJ/mol. This enhanced binding in the Ag_4 series is primarily driven by the electrostatic term, which becomes substantially more negative upon increasing the nuclearity of the Ag core. In parallel, the orbital interaction also strengthens, reflecting improved Ag–Mo covalent interactions and electronic delocalisation within the square Ag_4 rings. Despite the rise in Pauli repulsion, especially in **A37**, the dominant attractive contributions lead to a pronounced stabilisation of the tetranuclear assemblies.

For all gold complexes, the interaction between the Au cores and the metalloligand is highly

stabilising. The Au_3 species (**A15**, **A17**, and **A20**) display interaction energies around −5.0 MJ/mol, whereas the Au_4 derivatives (**A3**, **A9**, **A12**, and **A38**) reach significantly larger values between −7.4 and −7.7 MJ/mol. Electrostatic attraction is the leading stabilising factor in both series, but it is strongly reinforced in the Au_4 clusters. The orbital term also increases markedly with nuclearity, confirming a substantial covalent contribution associated with Au–Mo bonding and metal–metal cooperation. Although Pauli repulsion rises in the Au_4 species, the net effect remains highly favourable, yielding the most stable complexes in this family.

The Cu_3 complexes **A4** and **A34** exhibit interaction energies of about −4.87 MJ/mol, whereas the Cu_4 derivatives display a much broader but generally more stabilising range extending down to −7.51 MJ/mol. In all cases, electrostatic interactions dominate the attractive forces, supported by sizable orbital contributions that point to significant Cu–Mo covalent bonding. The larger Pauli repulsion observed in some Cu_4 systems is counterbalanced by the stronger electrostatic and orbital stabilisation, leading overall to enhanced binding in the tetranuclear clusters. Although the EDA results indicate that the tetranuclear systems generally exhibit stronger interaction energies with the metalloligand fragments, this does not exclude the existence of trinuclear Cu_3 rafts. The EDA analysis mainly describes the metal–ligand interactions and does not fully account for other factors such as geometric constraints and intrinsic Cu–Cu bonding preferences. These effects can stabilise the triangular Cu_3 arrangement, allowing it to exist as a viable and locally stable structural motif despite the greater stabilisation predicted for the tetranuclear systems.

The Ag_3 complexes **A32** and **A35** show interaction energies around −4.40 MJ/mol, while the Ag_4 clusters (**A5**, **A22**, **A25**, **A28**, and **A39**) are substantially more stabilised, with ΔE_{int} values approaching −6.9 MJ/mol. As in the other series, electrostatic attraction is the principal stabilising factor and increases significantly with the size of the silver core. This is accompanied by a marked rise in orbital stabilisation, evidencing enhanced Ag–Mo covalent interactions. Even though Pauli repulsion becomes larger in the Ag_4 clusters, the combined electrostatic and orbital effects clearly favor the tetranuclear species.

The Au_4 complexes (**A6**, **A23**, **A26**, **A30**, and **A40**) exhibit much more negative interaction energies (−7.3 to −7.6 MJ/mol) than the Au_3 species **A33** and **A36**, confirming the strong stabilising effect of increasing gold nuclearity. This enhanced binding is the result of both a stronger electrostatic attraction and a reinforced orbital interaction, indicating more effective Mo→Au donation and Au→Mo backdonation in the square Au_4 cores. Among them, **A23** and **A26** stand out by their particularly large orbital contributions, reflecting pronounced covalent character and efficient metal–metal electronic communication. Although Pauli repulsion is higher in the Au_4 systems, it is more than compensated by the dominant attractive interactions.

The EDA results also rationalise the higher stability of the tetranuclear Ag_4 and Au_4 clusters compared with their trinuclear analogues. The square M_4 cores provide a more favourable electronic environment that enables a more efficient charge redistribution between the metal core and the metalloligand fragments. Consequently, both the electrostatic ΔE_{elstat} and orbital ΔE_{orb} contributions become more stabilising when moving from M_3 to M_4 species. Although Pauli repulsion increases in the more compact M_4 structures, it is largely compensated by the stronger attractive interactions.

A clear and systematic trend is observed with increasing nuclearity of the metal core. For all three metals, the tetranuclear M_4 systems are significantly more stabilised than their trinuclear M_3 analogues. For Cu and Ag, the ΔE_{int} values increase from approximately −4.4 to −5.0 MJ/mol in the M_3 species to about −6.6 to −7.6 MJ/mol in the M_4 clusters, while for Au, the stabilisation increases from around −5.0 MJ/mol in Au_3 to nearly −7.7 MJ/mol in Au_4. This pronounced enhancement reflects the cooperative effect of adding a fourth metal centre, which enables a more efficient distribution of charge and stronger metal–ligand and metal–metal interactions within the square cores.

In all complexes, the electrostatic term ΔE_{elstat} represents the dominant attractive contribution, accounting for the largest fraction of the stabilisation. This highlights the strong Coulombic attraction between the positively charged coinage-metal cores and the anionic Mo-based metalloligand fragments. Importantly, ΔE_{elstat} becomes markedly more negative when moving from M_3 to M_4 systems,

indicating that the square arrangements provide a more favourable electrostatic environment for binding the four metalloligands around the metal core. The orbital interaction term ΔE_{orb} is also very large and systematically increases with nuclearity, revealing a substantial covalent component in the metal–ligand bonding. The much stronger ΔE_{orb} values in the M_4 complexes indicate enhanced Mo→M σ-donation and M→Mo π-back-donation, as well as more effective metal–metal electronic communication within the cyclic M_4 frameworks. This effect is particularly pronounced for the gold clusters, consistent with the well-known high polarisability and relativistic stabilisation of Au orbitals, which promote strong covalent and aurophilic interactions. Pauli repulsion ΔE_{Pauli} increases with the size and compactness of the metal core, especially in tetranuclear clusters, as a consequence of greater overlap between filled orbitals in crowded square geometries. Nevertheless, this destabilising contribution is systematically outweighed by the much larger electrostatic and orbital stabilisations. The steric term ΔE_{ster}, which combines Pauli repulsion and electrostatic interactions, remains overall favourable, further supporting the structural viability of these clusters.

Taken together, the EDA results demonstrate that the superior stability of the M_4 assemblies relative to the M_3 analogues arises from the cooperative interplay of strong electrostatic attraction, enhanced covalent metal–ligand bonding, and efficient metal–metal interactions within the square cores. This synergy explains the marked preference for tetranuclear Cu, Ag, and Au architectures in these Mo-based metalloligand systems and underlines the key role of nuclearity in tuning the bonding and stability of coinage-metal clusters.

3.6. *Frontier molecular orbital analysis*

The frontier molecular orbitals (FMOs), namely the highest occupied molecular orbital (HOMO) and the lowest unoccupied molecular orbital (LUMO), are fundamental to the electronic structure, chemical stability, and reactivity of molecular systems [50,51,55,56]. The HOMO reflects a molecule's electron-donating capability, whereas the LUMO indicates its electron-accepting potential. The energy separation between these two orbitals, commonly referred to as the HOMO–LUMO gap (ΔE), serves as an important descriptor of molecular stability and chemical reactivity. To visualise the electronic structure of clusters **A1**–**A42**, the HOMO and LUMO energy levels for the hydride complexes were plotted. The corresponding FMO distributions are presented in Figure 9 (see also Supplementary Figures S1–S6).

The FMOs provide essential insight into the electronic stability and reactivity of the Cu, Ag, and Au clusters investigated in this series (**A1**–**A42**). The calculated energy levels and HOMO–LUMO gaps clearly demonstrate that the nature of the metal, the presence of the electron-donating NMe_2 ligand, and the cluster nuclearity jointly govern the overall electronic behaviour. For all complexes, the HOMO corresponds to the highest doubly occupied molecular orbital and is predominantly metal-centred, with major contributions from the d orbitals of the coinage metal (Cu, Ag, or Au) and Mo, as well as varying participation from the Cp and $C_5H_4NMe_2$ ligands. The LUMO is systematically an unoccupied orbital dominated by Mo d and CO π^* contributions. Accordingly, the lowest-energy electronic excitation in all clusters corresponds to a metal/ligand-to-carbonyl charge-transfer (MLCT) process. The energy separation between these two orbitals, $\Delta E = E_{LUMO} - E_{HOMO}$, directly reflects the ease of electron promotion, redox activity, and electronic softness of the clusters. A dominant trend across all metal families is the influence of the NMe_2 substituent. In the substituted series $[MMo(C_5H_4NMe_2)(CO)_3]_n$ (M = Cu, Ag, Au), the HOMO is significantly destabilised relative to the unsubstituted $[MMoCp(CO)_3]_n$ analogues. This effect originates from the strong σ-donor character of the NMe_2 group, which injects electron density into the metal–Mo–Cp framework and increases the population of metal–ligand bonding orbitals. Consequently, the HOMO energies are shifted upward and the HOMO–LUMO gaps are reduced. This behaviour is clearly reflected in the orbital plots (Figures S1, S3, and S5), where the HOMO of the NMe_2-substituted clusters shows significant ligand participation in addition to metal d contributions. The resulting increase in electron density at the metal centres enhances back-donation to the carbonyl ligands and stabilises low-lying antibonding orbitals, bringing the LUMO closer in energy to the HOMO. As a result, the NMe_2 substituted clusters are more polarisable, electronically softer, and

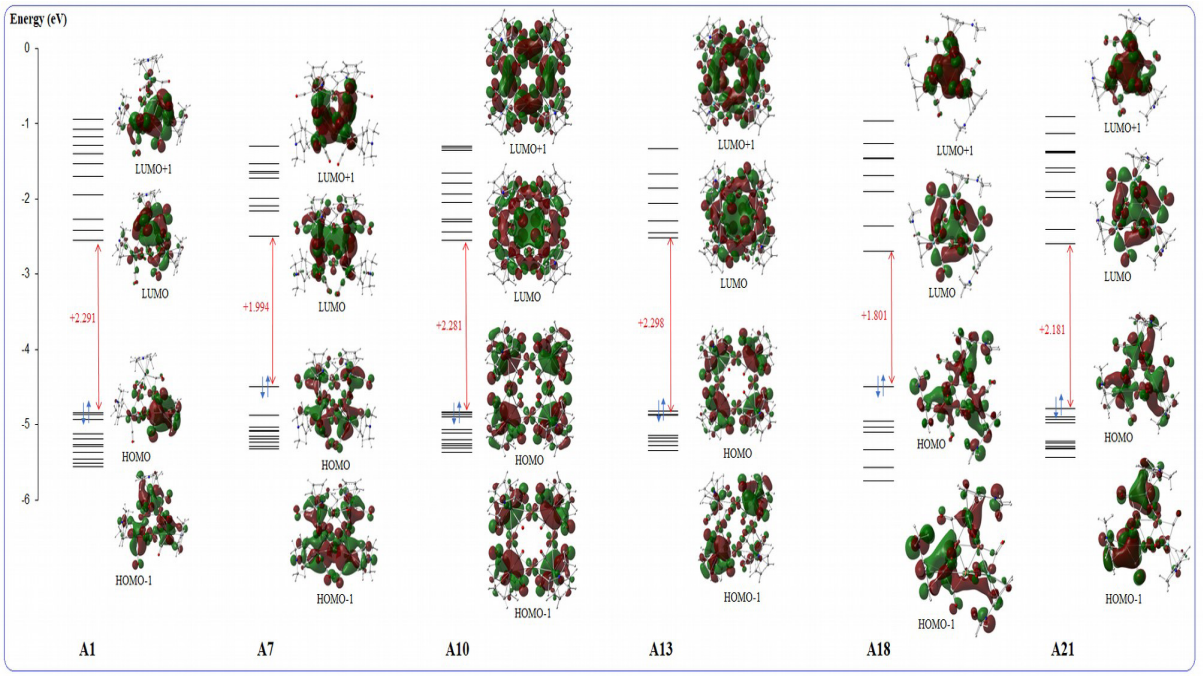

Figure 9. Molecular orbital energy (eV) of $[CuMo(C_5H_4NMe_2)(CO)_3]_n$ ($n = 3$ for **A1**, **A18**, **A21**, and $n = 4$ for **A7**, **A10**, **A13**).

chemically more reactive than their unsubstituted counterparts. Among the three coinage metals, Cu-based clusters exhibit the highest HOMO energies and the smallest HOMO–LUMO gaps, making them the most electronically active systems. In the substituted $[CuMo(C_5H_4NMe_2)(CO)_3]_n$ series, the HOMO lies in the range −4.49 to −4.84 eV, reflecting strong Cu–Mo and Cu–NMe_2 interactions. The HOMO is fully occupied and delocalised over the Cu–Mo core with substantial ligand contribution, indicating efficient electron donation from NMe_2 into metal-centred bonding orbitals. The corresponding LUMO is largely Mo–CO π^* in character and remains relatively low in energy (−2.49 to −2.69 eV), resulting in small HOMO–LUMO gaps (1.80–2.30 eV). In particular, **A18**, which exhibits the smallest gap, features a strongly delocalised HOMO and a low-lying LUMO, enabling facile MLCT transitions and high redox activity. In the unsubstituted $[CuMoCp(CO)_3]_n$ clusters, removal of the NMe_2 donor stabilises the HOMO (−4.83 to −5.29 eV) and leads to a concomitant increase in the energy gap. The HOMO becomes more localised on the metal–CO framework, while the LUMO retains its Mo–CO π^* character. This larger separation between occupied and virtual orbitals explains why these systems are more electronically robust but less reactive than their NMe_2-substituted counterparts. Replacing Cu with Ag leads to a pronounced increase in electronic stability. In $[AgMo(C_5H_4NMe_2)(CO)_3]_n$, the HOMO energies are lower than in the Cu analogues (−4.53 to −4.86 eV), while the LUMO levels remain relatively high (−2.19 to −2.43 eV), yielding HOMO–LUMO gaps of 2.14–2.64 eV. The HOMO in these systems is dominated by Ag–Mo d orbitals with limited ligand participation, reflecting weaker σ donation from NMe_2 compared with the Cu system. In the unsubstituted $[AgMoCp(CO)_3]_n$ series, the HOMO is further stabilised (−5.02 to −5.24 eV), whereas the LUMO remains Mo–CO π^* in character, resulting in the largest HOMO–LUMO gaps of the entire dataset (up to 2.73 eV for **A35**). The diffuse nature of the Ag 4d orbitals reduces metal–ligand overlap and promotes electron localisation, which is clearly visible in the FMO plots. Consequently, Ag-based clusters are calculated to be the most electronically stable and least reactive systems in this study. Au clusters display an intermediate electronic character

between Cu and Ag systems. In the NMe_2-substituted $[AuMo(C_5H_4NMe_2)(CO)_3]_n$ series, the HOMO spans a broad energy range (−4.25 to −5.20 eV), reflecting sensitivity to nuclearity and coordination environment. Relativistic stabilisation of the Au 5d orbitals enhances Au–Mo and Au–ligand covalency, leading to efficient electronic delocalisation. The LUMO remains dominated by Mo–CO π^* character, but for some complexes, notably **A9**, it lies unusually close to the HOMO, giving rise to a small gap (1.76 eV) and pronounced electronic softness. In the unsubstituted $[AuMoCp(CO)_3]_n$ family, two distinct regimes emerge. The $n = 4$ clusters display relatively small gaps (1.95–1.99 eV), consistent with strong delocalisation over the extended Au–Mo framework, whereas the $n = 3$ species exhibit much larger gaps (>2.45 eV), indicative of more localised electronic structures and higher stability. Across all metal families, increasing the nuclearity from $n = 3$ to $n = 4$ systematically reduces the HOMO–LUMO gap. The larger metal framework allows greater delocalisation of the HOMO over multiple metal centres and stabilises low-lying charge-transfer states. This effect is particularly pronounced for Au clusters but is also evident for Cu and Ag systems. Taken together, the FMO analysis shows that the HOMO is always a fully occupied metal–ligand bonding orbital, while the LUMO is a Mo–CO antibonding orbital. The HOMO→LUMO transition therefore corresponds to a MLCT process, which is most facile in Cu- and Au-based NMe_2-substituted clusters and in $n = 4$ species. These systems are thus predicted to be the most electronically soft, redox-active, and catalytically promising, whereas Ag-based and unsubstituted clusters, characterised by larger HOMO–LUMO gaps and more localised FMOs, are expected to be the most electronically stable and resistant to excitation.

4. Conclusion

Taking advantage of the full characterisation of a unique series of 2D raft-type heterometallic clusters, we could perform a systematic investigation of the energies and relative stabilities of Cu(I), Ag(I), and Au(I)-containing clusters with triangular and square core geometries under different symmetries (C_1, C_s, C_2, D_2, and S_4), which allowed a clear comparison with the experimentally determined X-ray structures. In the case of clusters bearing the Cp ligand, an excellent agreement was observed between theory and experiment, since the most stable computed structures corresponded closely to those reported crystallographically. With $C_5H_4NMe_2$ as π-ligand, our calculations indicated that alternative arrangements more stable than those experimentally observed are possible, thereby highlighting the significant effect of the π-ligand substitution on the overall stability and geometry of the clusters, although no direct interaction was observed between the NMe_2 group and the coinage metals. It is not too surprising to sometimes observe differences between calculated and experimental values involving the carbonyl ligands and the coinage metals, since the relevant interactions are much weaker than those involving the carbonyl ligands and molybdenum.

Furthermore, previously reported square copper clusters such as $[Et_4N]_4[M_4Cu_4S_{12}O_4]$ (M = Mo, W) [56] and $[(\eta^5\text{-}C_5Me_5)WS_3Cu]_4$ [57] exhibit elongated Cu–Cu distances, which are consistent with our theoretical findings since we found that square copper clusters with long Cu–Cu separations can indeed be stabilised. There is a subtle balance between stabilisation through electronic factors and destabilisation due to steric effects, while packing effects may also play a role.

The energy decomposition analysis provides a clear and quantitative understanding of the bonding mechanism in these coinage-metal clusters. In all systems, electrostatic attraction between the positively charged metal cores and the Mo-based metalloligands represents the dominant stabilising force, while large orbital interaction terms reveal a substantial covalent component associated with Mo→M donation and M→Mo back-donation. The markedly higher stabilisation observed for the tetranuclear M_4 (M = Cu, Ag, Au) complexes compared with their M_3 analogues demonstrates the cooperative nature of metal–metal and metal–ligand interactions within the square cores. These findings rationalise the enhanced stability of the M_4 architectures and highlight nuclearity as a key factor governing the electronic structure and bonding of metalloligand-stabilised coinage-metal clusters. The electronic properties of these clusters are controlled by a balance between metal type, ligand donation, and nuclearity. Cu- and Au-based $C_5H_4NMe_2$-substituted clusters, especially with $n = 4$, show enhanced delocalisation and superior charge-transfer capability. In contrast, Ag-based

and unsubstituted systems are more electronically stable and better suited for applications requiring robust molecular frameworks.

This work demonstrates that DFT calculations not only satisfactorily reproduce experimental findings but can also predict new, potentially accessible geometries, thereby offering valuable guidance for future experimental investigations.

Acknowledgements

The authors are grateful to Dr. Peter Deglmann (University of Heidelberg, Germany; now BASF SE, Ludwigshafen, Germany), for providing computer resources and continuous encouragement.

Declaration of interests

The authors do not work for, advise, own shares in, or receive funds from any organization that could benefit from this article, and have declared no affiliations other than their research organizations.

Supplementary materials

Supporting information for this article is available on the journal's website under https://doi.org/10.5802/crchim.448 or from the author.

References

[1] C. E. Coffey, J. Lewis and R. S. Nyholm, "339. Metal–metal bonds. Part I. Compounds of gold(0) with the carbonyls of manganese, iron, and cobalt", *J. Chem. Soc.* (1964), pp. 1741–1749.

[2] I. D. Salter, "Group IB metal exchange reactions: a novel, high yield route to heteronuclear cluster compounds containing M(PPh_3) (M = Cu, Ag or Au) moieties", *J. Organomet. Chem.* **295** (1985), pp. C17–C20.

[3] P. J. McCarthy, I. D. Salter and T. Adatia, "The heteronuclear cluster chemistry of the group IB metals, Part XVII. Synthesis and X-ray crystal structure of the hexanuclear mixed-metal cluster $[Ag_2Ru_4(\mu_3\text{-}H)_2(CO)_{12}\{P(C_6H_4Me\text{-}2)_3\}_2]$. An investigation of the steric properties of the $P(C_6H_4Me\text{-}2)_3$ ligand", *J. Organomet. Chem.* **485** (1995), pp. 191–199.

[4] V. Ritleng and M. J. Chetcuti, "Hydrocarbyl ligand transformations on heterobimetallic complexes", *Chem. Rev.* **107** (2007), pp. 797–858.

[5] P. Braunstein and A. A. Danopoulos, "Transition metal chain complexes supported by soft donor assembling ligands", *Chem. Rev.* **121** (2021), pp. 7346–7397.

[6] I. D. Salter, "Cluster complexes with bonds between transition elements and copper, silver and gold", in *Comprehensive Organometallic Chemistry II*, Elsevier: Amsterdam, 1995, pp. 255–322.

[7] P. Braunstein, L. A. Oro and P. R. Raithby, *Metal Clusters in Chemistry*, Wiley: Hoboken, NJ, 1999.

[8] P. Pyykkö, "Strong closed-shell interactions in inorganic chemistry", *Chem. Rev.* **97** (1997), pp. 597–636.

[9] X. He and V. W.-W. Yam, "Luminescent gold(I) complexes for chemosensing", *Coord. Chem. Rev.* **255** (2011), pp. 2111–2123.

[10] M. J. Katz, K. Sakai and D. B. Leznoff, "The use of aurophilic and other metal–metal interactions as crystal engineering design elements to increase structural dimensionality", *Chem. Soc. Rev.* **37** (2008), pp. 1884–1895.

[11] T. E. Karpiuk, R. Y. Williams-Sekiguchi, S. Mahato, T. Storr and D. B. Leznoff, "A shape-complementarity approach to inducing short Au(III)$\cdots$Au(III) contacts in tetracyanoaurate(III) salts", *Chem.–A Eur. J.* **31** (2025), article no. e202501685.

[12] H. Schmidbaur and A. Schier, "A briefing on aurophilicity", *Chem. Soc. Rev.* **37** (2008), pp. 1931–1951.

[13] H. Schmidbaur and A. Schier, "Argentophilic interactions", *Angew. Chem. Int. Ed.* **54** (2015), pp. 746–784.

[14] Y.-J. Wang, X.-Y. Shi, P. Xing and S.-Q. Zang, "Metallophilic interactions drive supramolecular chirality evolution and amplify circularly polarized luminescence", *JACS Au* **3** (2023), pp. 565–574.

[15] C. Cesari, C. Femoni, F. Forti, M. C. Iapalucci, G. Scorzoni and S. Zacchini, "Isomerism in molecular metal carbonyl clusters", *Eur. J. Inorg. Chem.* **27** (2024), article no. e202400220.

[16] X.-M. Luo, Y.-K. Li, X.-Y. Dong and S.-Q. Zang, "Platonic and archimedean solids in discrete metal-containing clusters", *Chem. Soc. Rev.* **52** (2023), pp. 383–444.

[17] S. Sculfort and P. Braunstein, "Intramolecular d^{10}–d^{10} interactions in heterometallic clusters of the transition metals", *Chem. Soc. Rev.* **40** (2011), pp. 2741–2760.

[18] V. G. Albano, F. Azzaroni, M. C. Iapalucci, G. Longoni, M. Monari, S. Mulley, D. M. Proserpio and A. Sironi, "Synthesis, chemical characterization, and bonding analysis of the $[Ag\{Fe(CO)_4\}_2]^{3-}$, $[Ag_4\{\mu_2\text{-}Fe(CO)_4\}_4]^{4-}$, and $[Ag_5\{\mu_2\text{-}Fe(CO)_4\}_2\{\mu_3\text{-}Fe(CO)_4\}_2]^{3-}$ cluster anions. X-ray structural determination of $[NMe_3CH_2Ph]_4[Ag_4Fe_4(CO)_{16}]$ and $[NEt_4]_3[Ag_5Fe_4(CO)_{16}]$", *Inorg. Chem.* **33** (1994), pp. 5320–5328.

[19] V. G. Albano, F. Calderoni, M. C. Lapalucci, G. Longoni and M. Monari, "Synthesis of $[AuFe_2(CO)_8]^{3-}$ and $[Au_4Fe_4(CO)_{16}]^{4-}$: X-ray structure of the $[Au_4Fe_4(CO)_{16}]^{4-}$ cluster anion in its $[NEt_4]^+$ salt", *J. Chem. Soc. Chem. Commun.* (1995), pp. 433–434.

[20] P. Klüfers, "Preparation and crystal structure of $CuCo(CO)_4$: a carbonylheterometal complex containing a Cu_4Co_4-ring", *Angew. Chem. Int. Ed. Engl.* **23** (1984), pp. 307–308.

[21] P. Klüfers, "Die Kristallstruktur von $AgCo(CO)_4$", *Z. Kristallogr.—Cryst. Mater.* **166** (1984), pp. 143–152.

[22] P. Klüfers, "$[CuCo(CO)_4]_n$—crystal structure of a polymer with a one-dimensional, infinite copper-cobalt bonding system", *Angew. Chem. Int. Ed. Engl.* **24** (1985), pp. 70–71.

[23] G. Doyle, K. A. Eriksen and D. Van Engen, "Mixed copper/iron clusters. The preparation and structure of the large planar cluster anions, $Cu_3Fe_3(CO)_{12}^{3-}$ and $Cu_5Fe_4(CO)_{16}^{3-}$ ", *J. Am. Chem. Soc.* **108** (1986), pp. 445–451.

[24] B. Berti, M. Bortoluzzi, C. Cesari, C. Femoni, M. C. Iapalucci, R. Mazzoni, F. Vacca and S. Zacchini, "Polymerization Isomerism in $[\{MFe(CO)_4\}_n]^{n-}$ (M = Cu, Ag, Au; n = 3, 4) molecular clusters supported by metallophilic interactions", *Inorg. Chem.* **58** (2019), pp. 2911–2915.

[25] S. Sculfort, P. Croizat, A. Messaoudi, M. Bénard, M.-M. Rohmer, R. Welter and P. Braunstein, "Two-dimensional triangular and square heterometallic clusters: influence of the closed-shell d^{10} electronic configuration", *Angew. Chem.—Int. Ed.* **48** (2009), pp. 9663–9667.

[26] P. Croizat, S. Sculfort, R. Welter and P. Braunstein, "Hexa- and octanuclear heterometallic clusters with copper–, silver–, or gold–molybdenum bonds and d^{10}–d^{10} interactions", *Organometallics* **35** (2016), pp. 3949–3958.

[27] S. Sculfort, R. Welter and P. Braunstein, "Heterometallic chains and clusters with gold-transition metal bonds: synthesis and interconversion", *Inorg. Chem.* **49** (2010), pp. 2372–2382.

[28] N. Auvray, T. S. Basu Baul, P. Braunstein, P. Croizat, U. Englert, G. E. Herberich and R. Welter, "Organometallic building blocks with amino-substituted cyclopentadienyl and boratabenzene ligands for the synthesis of heterometallic complexes and clusters", *Dalton Trans.* (2006), pp. 2950–2958.

[29] R. Bender, P. Braunstein, Y. Dusausoy and J. Protas, "Preparation and crystal structure of $Pd_2Mo_2(\eta^5\text{-}C_5H_5)_2(\mu_3\text{-}CO)_2(\mu_2\text{-}CO)_4(PEt_3)_2$. A planar, triangulated, palladium-molybdenum-carbonyl cluster", *Angew. Chem. Int. Ed. Engl.* **17** (1978), pp. 596–597.

[30] R. Bender, P. Braunstein, J. M. Jud and Y. Dusausoy, "Organometallic complexes with metal-metal bonds. 18. Syntheses of tetrametallic planar, triangulated mixed-metal palladium clusters. X-ray crystal structures of $Pd_2M_2(\eta^5\text{-}C_5H_5)_2(\mu_3\text{-}CO)_2(\mu_2\text{-}CO)_4(PEt_3)_2$ with M = Cr, Mo, and W", *Inorg. Chem.* **22** (1983), pp. 3394–3407.

[31] R. Bender, P. Braunstein, J. M. Jud and Y. Dusausoy, "Organometallic complexes with metal-metal bonds. 19. Comparison of two strategies towards the syntheses of platinum mixed-metal clusters. Reactivity of linear M–Pt–M and Mn–Pt–Mn complexes. X-ray crystal structures of $Pt_2M_2(\mu^5\text{-}C_5H_5)_2(\mu_3\text{-}CO)_2(\mu\text{-}CO)_4(PEt_3)_2$ with M = Cr, Mo, and W", *Inorg. Chem.* **23** (1984), pp. 4489–4502.

[32] K. Wade, "The structural significance of the number of skeletal bonding electron-pairs in carboranes, the higher boranes and borane anions, and various transition-metal carbonyl cluster compounds", *J. Chem. Soc. D: Chem. Commun.* (1971), pp. 792–793.

[33] D. M. P. Mingos, "A general theory for cluster and ring compounds of the main group and transition elements", *Nat. Phys. Sci.* **236** (1972), pp. 99–102.

[34] P. Braunstein, J. Fischer, D. Matt and M. Pfeffer, "Relevance to synthetic polynuclear chemistry of novel μ_3-coordination modes for the anions $[Ph_2PCHC(O)OC_2H_5]^-$ and $[Mo(CO)_3Cp]^-$. Synthesis and X-ray structure of $Pd(8\text{-mq})Br[Ph_2PCH_2C(O)OC_2H_5]$, $[\{Pd(8\text{-mq})\}_3\{\mu_3\text{-}Ph_2PCHC(O)OC_2H_5\}(\mu_3\text{-}OH)]PF_6$ and $\{[Pd(8\text{-mq})]_3[\mu_3\text{-}Mo(CO)_3Cp](\mu_3\text{-}Cl)\}BF_4$", *J. Am. Chem. Soc.* **106** (1984), pp. 410–421.

[35] N. Naili, S. Kahlal, B. Zouchoune, J. Saillard and P. Braunstein, "Carbonylmetallates as versatile 2-, 4- or 6-electron donor metalloligands in transition- metal complexes and clusters: a global approach", *Chem. – A Eur. J.* **29** (2023), article no. e202203557.

[36] R. Ahlrichs, M. Bär, M. Häser, H. Horn and C. Kölmel, "Electronic structure calculations on workstation computers: The program system turbomole", *Chem. Phys. Lett.* **162** (1989), pp. 165–169.

[37] A. D. Becke, "Density-functional exchange-energy approximation with correct asymptotic behavior", *Phys. Rev. A (Coll Park)* **38** (1988), pp. 3098–3100.

[38] S. H. Vosko, L. Wilk and M. Nusair, "Accurate spin-dependent electron liquid correlation energies for local spin density calculations: a critical analysis", *Can. J. Phys.* **58** (1980), pp. 1200–1211.

[39] J. P. Perdew, "Density-functional approximation for the correlation energy of the inhomogeneous electron gas", *Phys. Rev. B* **33** (1986), pp. 8822–8824.

[40] K. Eichkorn, F. Weigend, O. Treutler and R. Ahlrichs, "Auxiliary basis sets for main row atoms and transition metals and their use to approximate Coulomb potentials", *Theor. Chem. Acc.: Theory Comput. Model. (Theor. Chim. Acta)* **97** (1997), pp. 119–124.

[41] K. Eichkorn, O. Treutler, H. Öhm, M. Häser and R. Ahlrichs, "Auxiliary basis sets to approximate Coulomb potentials", *Chem. Phys. Lett.* **240** (1995), pp. 283–290.

[42] A. Schäfer, H. Horn and R. Ahlrichs, "Fully optimized contracted Gaussian basis sets for atoms Li to Kr", *J. Chem. Phys.* **97** (1992), pp. 2571–2577.

[43] A. Schäfer, C. Huber and R. Ahlrichs, "Fully optimized contracted Gaussian basis sets of triple zeta valence quality for atoms Li to Kr", *J. Chem. Phys.* **100** (1994), pp. 5829–5835.

[44] P. Deglmann, F. Furche and R. Ahlrichs, "An efficient implementation of second analytical derivatives for density functional methods", *Chem. Phys. Lett.* **362** (2002), pp. 511–518.

[45] A. Messaoudi, P. Deglmann, P. Braunstein and P. Hofmann, "Investigations on a novel silyl transfer reaction in heterodimetallic chemistry", *Inorg. Chem.* **46** (2007), pp. 7899–7909.

[46] P. Deglmann, K. May, F. Furche and R. Ahlrichs, "Nuclear second analytical derivative calculations using auxiliary basis set expansions", *Chem. Phys. Lett.* **384** (2004), pp. 103–107.

[47] K. Morokuma, "Molecular orbital studies of hydrogen bonds. III. C =O··· H–O hydrogen bond in $H_2CO\cdots H_2O$ and $H_2CO\cdots 2H_2O$", *J. Chem. Phys.* **55** (1971), pp. 1236–1244.

[48] E. J. Baerends, N. F. Aguirre, N. D. Austin, et al., "The amsterdam modeling suite", *J. Chem. Phys.* **162** (2025), no. 16, article no. 162501.

[49] A. Messaoudi, "Structure, electronic, vibrational, and NLO properties of thiolato-bridged diruthenium cations: A computational study", *J. Organomet. Chem.* **1043** (2026), article no. 123911.

[50] A. Messaoudi, "Electronic structure and reactivity of mixed-ligand dinuclear Ru Ir, Ru Rh, and Ru Ru polyhydride-bridged complexes: a DFT-based investigation", *Polyhedron* **285** (2026), article no. 117909.

[51] H. Maddi, A. Messaoudi, O. Khaoua, A. Midoune and N. Benbellat, "Exploration of transition metal-hydride compounds: molecular structure, electronic properties, nonlinear optical characteristics, and reactivity of Cp-based binuclear ruthenium complexes", *J. Organomet. Chem.* **1036** (2025), article no. 123709.

[52] M. J. Frisch, G. W. Trucks, H. B. Schlegel, et al., *Gaussian 16*, Gaussian, Inc.: Wallingford, CT, 2019.

[53] M. Iliaš and V. Pershina, "Hexacarbonyls of Mo, W, and Sg: metal–CO bonding revisited", *Inorg. Chem.* **56** (2017), pp. 1638–1645.

[54] G. Manca and A. Messaoudi, "A potential case of the rare cluster core isomerism for phosphido-bridged Pt_3 units suggested by DFT calculations", *Inorg. Chim. Acta* **470** (2018), pp. 439–444.

[55] R. Hoffmann, S. Alvarez, C. Mealli, A. Falceto, T. J. Cahill, T. Zeng and G. Manca, "From widely accepted concepts in coordination chemistry to inverted ligand fields", *Chem. Rev.* **116** (2016), pp. 8173–8192.

[56] Q. Huang, X. Wu, Q. Wang, T. Sheng and J. Lu, "Heterobimetallic clusters of copper(I) with trithiotungstate and trithiomolybdate. Synthesis and characterization of the octanuclear clusters $[Et_4N]_4[M_4Cu_4S_{12}O_4]$ (M = Mo, W) and the dodecanuclear clusters $[M_4Cu_4S_{12}O_4(CuTMEN)_4]$ (M = Mo, W; TMEN = *N*, *N*, *N*′, *N*′-tetramethylethylenediamine)", *Inorg. Chem.* **35** (1996), pp. 893–897.

[57] J.-P. Lang and K. Tatsumi, "Reactions of $[PPh_4][(\eta^5\text{-}C_5Me_5)WS_3]$ with CuBr in $CHCl_3$: isolation and structures of an octanuclear cluster $[(\eta^5\text{-}C_5Me_5)WS_3Cu]_4$ and a trinuclear cluster $[(\eta^5\text{-}C_5Me_5)WS_3Cu_2Br(PPh_3)_2]$", *J. Organomet. Chem.* **579** (1999), pp. 332–337.